Available online at www.sciencedirect.com
SCIENCE DIRECT®
Chemie der Erde 64 (2004) 185–239
CHEMIE der ERDE GEOCHEMISTRY
www.elsevier.de/chemer

INVITED REVIEW

Amoeboid olivine aggregates and related objects in carbonaceous chondrites: records of nebular and asteroid processes

Alexander N. Krot[a,*], Michail I. Petaev[b], Sara S. Russell[c], Shoichi Itoh[c,d], Timothy J. Fagan[d,e], Hisayoshi Yurimoto[d], Lysa Chizmadia[f], Michael K. Weisberg[g,h], Matsumi Komatsu[i], Alexander A. Ulyanov[j], Klaus Keil[a]

[a] *School of Ocean and Earth Science and Technology, Hawaii Institute of Geophysics and Planetology, University of Hawaii at Manoa, Honolulu, HI 96822, USA*
[b] *Department of Earth and Planetary Sciences, Harvard-Smithsonian Center for Astrophysics, Harvard University, Cambridge, MA 02138, USA*
[c] *Department of Mineralogy, The Natural History Museum, Cromwell Road, London SW7 5BD, UK*
[d] *Department of Earth and Planetary Sciences, Tokyo Institute of Technology, Tokyo 152-8551, Japan*
[e] *Department of Mineral Sciences, Smithsonian Institution, NHB 119, Washington DC 20560, USA*
[f] *Department of Earth and Planetary Sciences, University of New Mexico, Albuquerque, NM 87131, USA*
[g] *Department of Physical Sciences, Kingsborough College of the City University of New York, Brooklyn, NY 11235, USA*
[h] *Earth and Planetary Science Department, American Museum of Natural History, Central Park West, NY 11235, USA*
[i] *The University Museum, University of Tokyo, Tokyo 113-033, Japan*
[j] *Department of Geology, Moscow State University, Moscow 119899, Russia*

Received 30 January 2004; accepted 14 May 2004

*Corresponding author.
E-mail address: sasha@higp.hawaii.edu (A.N. Krot).

0009-2819/$ - see front matter © 2004 Elsevier GmbH. All rights reserved.
doi:10.1016/j.chemer.2004.05.001

Abstract

Amoeboid olivine aggregates (AOAs) are the most common type of refractory inclusions in CM, CR, CH, CV, CO, and ungrouped carbonaceous chondrites Acfer 094 and Adelaide; only one AOA was found in the CB_b chondrite Hammadah al Hamra 237 and none were observed in the CB_a chondrites Bencubbin, Gujba, and Weatherford. In primitive (unaltered and unmetamorphosed) carbonaceous chondrites, AOAs consist of forsterite ($Fa_{<2}$), Fe, Ni-metal (5–12 wt% Ni), and Ca, Al-rich inclusions (CAIs) composed of Al-diopside, spinel, anorthite, and very rare melilite. Melilite is typically replaced by a fine-grained mixture of spinel, Al-diopside, and $\pm$anorthite; spinel is replaced by anorthite. About 10% of AOAs contain low-Ca pyroxene replacing forsterite. Forsterite and spinel are always ^{16}O-rich ($\delta^{17,18}O \sim -40‰$ to $-50‰$), whereas melilite, anorthite, and diopside could be either similarly ^{16}O-rich or ^{16}O-depleted to varying degrees; the latter is common in AOAs from altered and metamorphosed carbonaceous chondrites such as some CVs and COs. Low-Ca pyroxene is either ^{16}O-rich ($\delta^{17,18}O \sim -40‰$) or ^{16}O-poor ($\delta^{17,18}O \sim 0‰$). Most AOAs in CV chondrites have unfractionated ($\sim 2–10 \times CI$) rare-earth element patterns. AOAs have similar textures, mineralogy and oxygen isotopic compositions to those of forsterite-rich accretionary rims surrounding different types of CAIs (compact and fluffy Type A, Type B, and fine-grained, spinel-rich) in CV and CR chondrites. AOAs in primitive carbonaceous chondrites show no evidence for alteration and thermal metamorphism. Secondary minerals in AOAs from CR, CM, and CO, and CV chondrites are similar to those in chondrules, CAIs, and matrices of their host meteorites and include phyllosilicates, magnetite, carbonates, nepheline, sodalite, grossular, wollastonite, hedenbergite, andradite, and ferrous olivine.

Our observations and a thermodynamic analysis suggest that AOAs and forsterite-rich accretionary rims formed in ^{16}O-rich gaseous reservoirs, probably in the CAI-forming region(s), as aggregates of solar nebular condensates originally composed of forsterite, Fe, Ni-metal, and CAIs. Some of the CAIs were melted prior to aggregation into AOAs and experienced formation of Wark-Lovering rims. Before and possibly after the aggregation, melilite and spinel in CAIs reacted with SiO and Mg of the solar nebula gas enriched in ^{16}O to form Al-diopside and anorthite. Forsterite in some AOAs reacted with ^{16}O-enriched SiO gas to form low-Ca pyroxene. Some other AOAs were either reheated in ^{16}O-poor gaseous reservoirs or coated by ^{16}O-depleted pyroxene-rich dust and melted to varying degrees, possibly during chondrule formation. The most extensively melted AOAs experienced oxygen isotope exchange with ^{16}O-poor nebular gas and may have been transformed into magnesian (Type I) chondrules. Secondary mineralization and at least some of the oxygen isotope exchange in AOAs from altered and metamorphosed chondrites must have resulted from alteration in the presence of aqueous solutions after aggregation and lithification of the chondrite parent asteroids.
© 2004 Elsevier GmbH. All rights reserved.

Keywords: Amoeboid olivine aggregates; Ca–Al-rich inclusions; Chondrules; Oxygen isotopes; Al–Mg system; Carbonaceous chondrites; Condensation; Alteration

1. Introduction

Amoeboid olivine aggregates (AOAs) are an important class of refractory objects originally recognized in the CV carbonaceous chondrite Allende by Grossman and

Steele (1976). AOAs are genetically related to Ca, Al-rich inclusions (CAIs) and are the dominant type of refractory inclusions in most carbonaceous chondrite groups (e.g., Weber and Bischoff, 1997; Krot et al., 2002a). They appear to have escaped extensive melting and must have preserved evidence for condensation from solar nebula gas, potentially providing unique information of physicochemical conditions [pressure (P), temperature (T), and oxygen fugacity (fO_2)] and isotopic composition of this gas (e.g., Krot et al., 2002b). In contrast, it is generally difficult to discriminate the effects of condensation, melting, and evaporation in CAIs (e.g., MacPherson et al., 1988; Krot et al., 2001a; Simon et al., 2002). Finally, AOAs are the least refractory of the refractory inclusions being chemically closer to magnesian chondrules than other refractory inclusions, providing a possible link between CAIs and chondrules. In spite of these unique features, AOAs have not yet received wide and detailed attention as objects of critical importance among cosmochemists.

In this paper, we summarize mineralogical, chemical and isotopic (oxygen and ^{26}Al–^{26}Mg) data from AOAs and forsterite-rich accretionary rims around CAIs in CM, CR, CH, CB, CV, CO, and ungrouped carbonaceous chondrites Acfer 094 and Adelaide. Because CK chondrites experienced extensive thermal metamorphism and no systematic studies of CK AOAs have yet been reported, they are not discussed here. We also carry out a thermodynamic analysis of high-temperature nebular condensation reactions and summarize evidence for a low-temperature asteroid processing recorded by AOAs and forsterite-rich accretionary rims, and discuss genetic relationships between AOAs, forsterite-rich accretionary rims and CAIs as well as between AOAs and magnesian chondrules. Finally, we outline suggestions for future studies of AOAs.

2. Results

2.1. AOAs in CV chondrites

CV (Vigarano-type) chondrites are a mineralogically diverse group of meteorites, which were divided by McSween (1977) into reduced and oxidized subgroups. The oxidized subgroup was subdivided further by Weisberg et al. (1997) into the Allende-like (CV_{oxA}) and Bali-like (CV_{oxB}) subgroups. Krot et al. (1998a, b) showed that the major differences between the Bali-like and Allende-like subgroups are due to the secondary, late-stage alteration. In both subgroups, common secondary minerals in chondrules, CAIs, and matrices include magnetite, Ni-rich metal, Fe, Ni-sulfides, Ca, Fe-rich pyroxenes, and andradite. Phyllosilicates and fayalite ($Fa_{>90}$) are common in the CV_{oxB} (e.g., Bali, Kaba, Mokoia), whereas secondary fayalitic olivine ($Fa_{30–50}$), nepheline and sodalite are observed largely in the CV_{oxA} (e.g., ALH84028, Allende). Secondary minerals in the reduced CV chondrites Efremovka and Leoville are similar to those in the CV_{oxA}, but much less abundant.

2.1.1. AOAs in the allende-like oxidized CV chondrites

2.1.1.1. Mineralogy and petrology. AOAs as a class of objects were originally defined in the Allende meteorite by Grossman and Steele (1976) and subsequently studied by Bar-Matthews et al. (1979), Grossman et al. (1979), Kornacki and Wood (1984a, b), and Hashimoto and Grossman (1987). In this section, we summarize the major results of these studies.

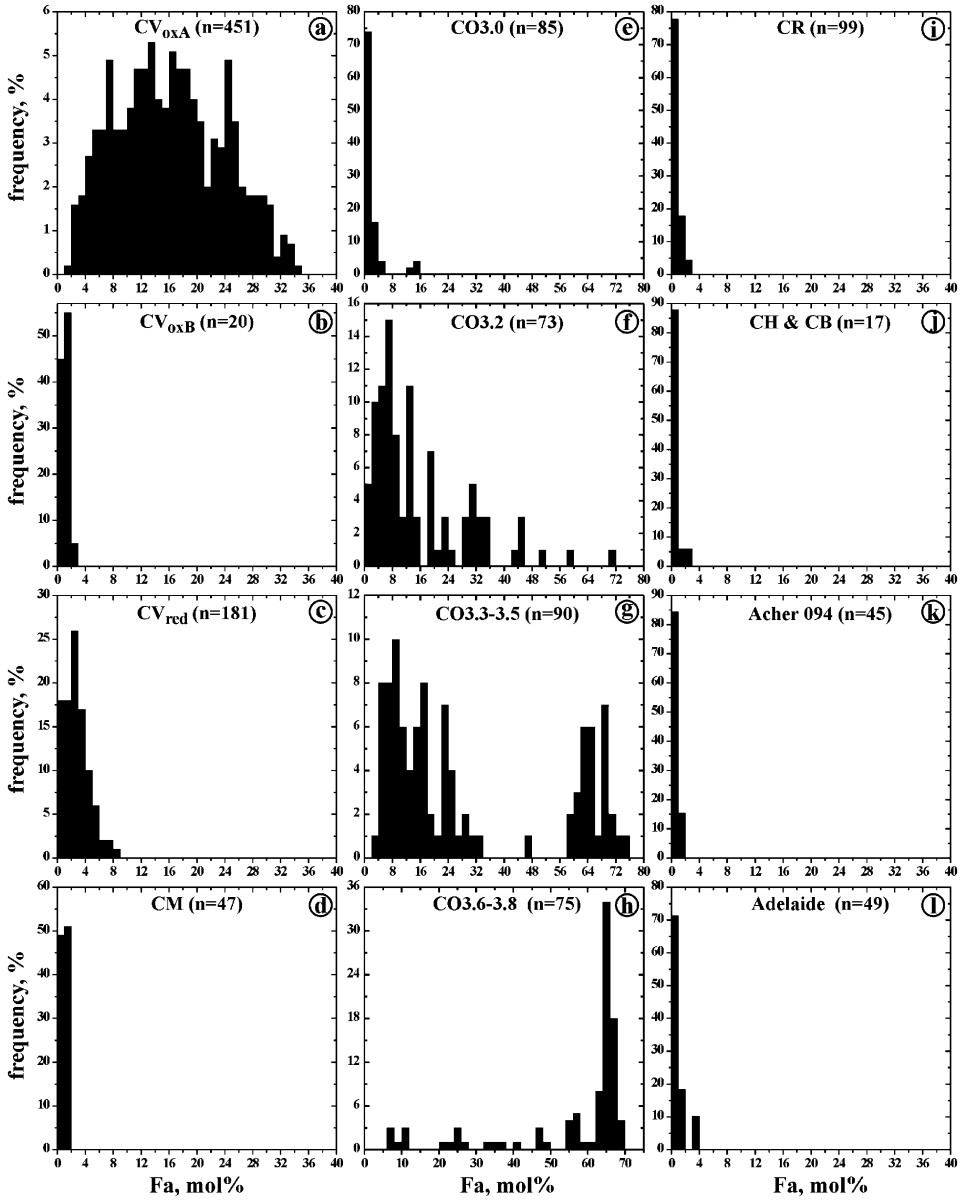
The Allende AOAs consist of olivine, high-Ca pyroxenes, nepheline, and sodalite; anorthite, spinel and perovskite are rare; melilite is generally absent. Olivine ranges in composition from Fo_{64-99}, with a peak at $\sim Fo_{80-85}$ (Fig. 1a); pyroxenes range from Al, Ti-diopside to hedenbergite; spinel contains 2–13 wt% FeO. Grossman and Steele (1976) concluded that perovskite, spinel, forsteritic olivine and Al, Ti-pyroxenes condensed from the nebular gas in the temperature range 1400–1600 K; some of these grains continued to equilibrate with the nebular vapor as it cooled to $\sim$900–500 K to form fayalitic olivine, nepheline and sodalite. Subsequent accretion of these micron-size grains resulted in the formation of subspherical clumps. Prior to aggregation of the clumps into AOAs, some of them were coated by a layer of coarser-grained forsterite condensed from the hot nebular gas.

Later, Hashimoto and Grossman (1987) showed that CAIs in Allende AOAs form an alteration sequence and concluded that alteration occurred in the solar nebula after aggregation of high-temperature condensates. During the alteration, melilite was replaced by anorthite + grossular; subsequently, anorthite was replaced by nepheline + sodalite; perovskite by ilmenite; Al, Ti-diopside and spinel by phyllosilicates.

Kornacki and Wood (1984a, b) divided Allende AOAs into rimmed and unrimmed types. The rimmed AOAs are aggregates of subrounded objects, each of which has a shell of granular olivine with grain boundaries forming 120° triple junctions. Rimmed AOAs are characterized by a wider compositional range of olivine than the unrimmed AOAs (Fo_{53-96} vs. Fo_{50-65}). Both types are mineralogically similar to the Allende matrix, but are depleted in Fe, Ni-metal and sulfides.

Fig. 1. Compositions of olivine in AOAs from (a) Allende (CV_{oxA}), (b) Kaba (CV_{oxB}), (c) Efremovka, Leoville, and Vigarano (CV_{red}), (d) Murchison (CM), (e–h) CO chondrites: (e) ALHA77307 (3.0), Y-81020 (3.0) and Colony (3.0), (f) Kainsaz (3.2), Y-82050 (3.2), and Rainbow (3.2), (g) Felix (3.3), Ornans (3.4), and Lance (3.5), and (h) ALHA77003 (3.6), Warrenton (3.7) and Isna (3.8), (i) CR chondrites, (j) NWA 739 and NWA 770 (CH) and Hammadah al Hamra 237 (CB_b), (k) Acfer 094 (ungrouped), and (l) Adelaide (ungrouped) carbonaceous chondrites. Olivines in AOAs from CV_{oxB}, CO3.0, CM, CR, CH, CB, Adelaide, and Acfer 094 are magnesium-rich compared to those from the CV_{red}, CO 3.2–3.8 and CV_{oxA} AOAs. In CO AOAs, enrichment of olivine in fayalite component is correlated with petrologic subtype of a host meteorite. Data for Allende are from Hashimoto and Grossman (1987), for Efremovka, Leoville, and Vigarano from Komatsu et al. (2000), for Acfer 094, Adelaide and CR from Aléon et al. (2002) and Krot et al. (2004a, unpublished), for CO from Chizmadia et al. (2002). *n*—number of analyses.

Kornacki and Wood (1984a, b) suggested that AOAs are aggregates of non-equilibrium condensates from supercooled gas in a relatively oxidizing, dust-rich parcel of interstellar material; rimmed AOAs formed during the solid-state recrystallization and incipient melting of unrimmed AOAs in the solar nebula.



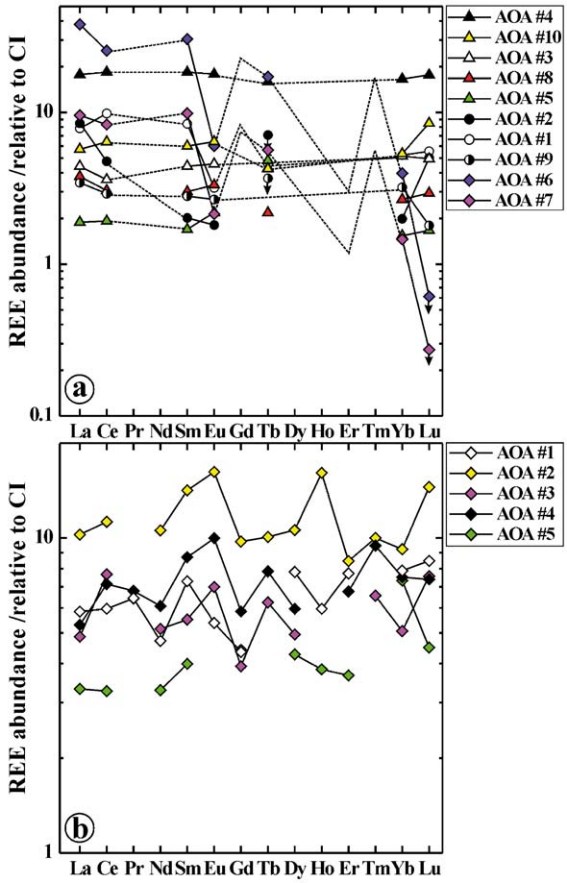


Fig. 2. Bulk rare-earth element abundances in AOAs from (a) CV_{oxA} Allende (data from Grossman et al., 1979), and (b) CV_{red} Efremovka (data from Russell et al., 2003).

Subsequently, both varieties of AOAs experienced Fe/Mg exchange in the Allende meteorite parent body.

2.1.1.2. Trace elements. Grossman et al. (1979) found that most Allende AOAs have unfractionated abundances of refractory lithophile and siderophile elements ($2–20 \times$ CI); two of the AOAs analyzed (♯6 and ♯7) have Group II REE patterns (Fig. 2a). They concluded that AOAs formed as a mixture of forsterite and refractory materials, some with fractionated and some with unfractionated REE patterns.

2.1.1.3. Oxygen isotopic compositions. The first measurements of oxygen isotopic compositions of density mineral separates from Allende AOAs (Clayton et al., 1977)

revealed small enrichments of olivine in ^{16}O relative to nepheline and sodalite ($\Delta^{17}O \sim -10‰$ and $-7‰$, respectively). Subsequent ion microprobe studies of AOAs in the CV_{oxA} chondrite Y-86009 by Hiyagon and Hashimoto (1999a) demonstrated that forsterite, spinel, diopside and fassaite (Al, Ti-diopside) are ^{16}O-enriched to a level commonly observed in spinel, hibonite and fassaite of the Allende CAIs ($\Delta^{17}O < -20‰$; Fig. 3a).

Recently, Imai and Yurimoto (2003) showed that olivine and refractory inclusions in Allende AOAs exhibit oxygen isotopic heterogeneity. Oxygen isotopic

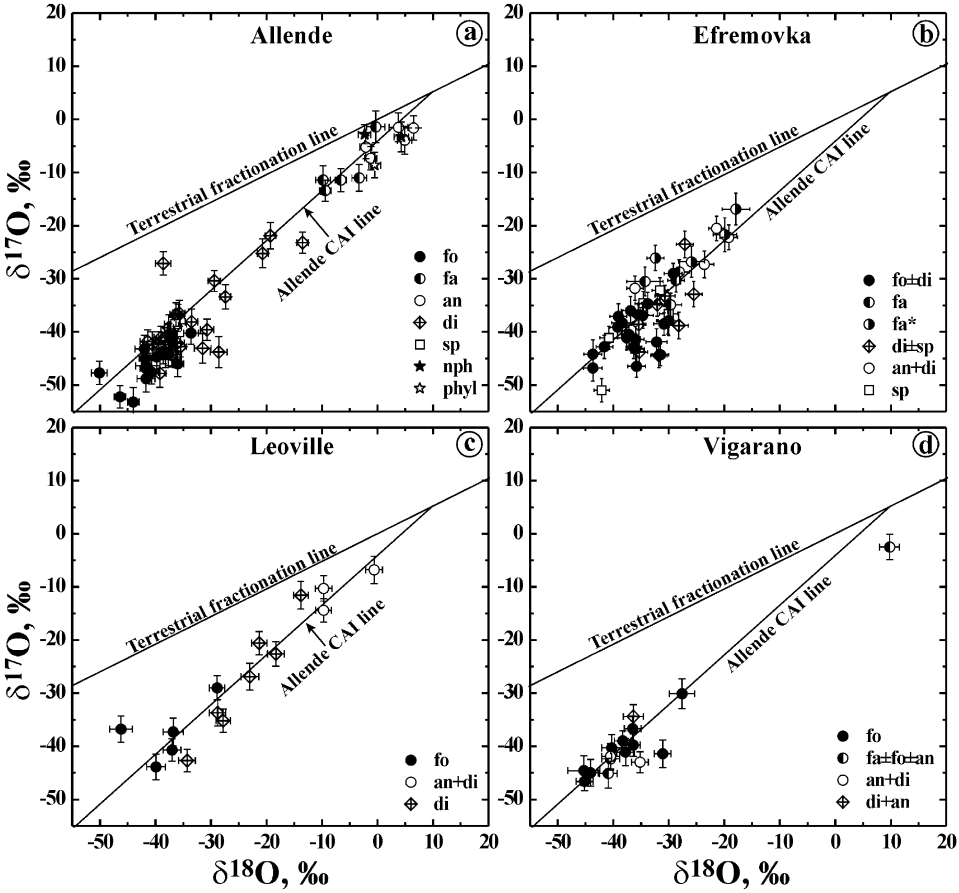


Fig. 3. Oxygen isotopic compositions (errors are 1σ) of individual minerals in AOAs from the (a) CV_{oxA} chondrite Allende (data from Imai and Yurimoto, 2003) and reduced CV chondrites (b) Efremovka, (c) Leoville, and (d) Vigarano (data from Fagan et al., 2003). Forsterite, spinel, and Al-diopside are ^{16}O-enriched relative to anorthite and secondary ferrous olivine, nepheline, and phyllosilicates. Terrestrial fractionation line and Allende CAI line are shown for references. an—anorthite, di—Al-diopside, fa—ferrous olivine, fa*—ferrous olivine with OH, fo—forsterite, nph—nepheline, phyl—phyllosilicates, and sp—spinel.

compositions of magnesian olivine (Fo_{95}) are ^{16}O-rich ($\Delta^{17}O \sim -25‰$), whereas those of ferrous olivine (Fo_{60}) are ^{16}O-poor ($\Delta^{17}O \sim -5‰$) (Fig. 3a). Oxygen isotopic compositions of spinel and Al, Ti-diopside are ^{16}O-rich ($\Delta^{17}O \sim -20‰$), whereas those of anorthite, nepheline, and phyllosilicates are ^{16}O-poor ($\Delta^{17}O \sim -5‰$). Imai and Yurimoto (2003) concluded that the alteration features and ^{16}O-poor compositions of anorthite and secondary nepheline, phyllosilicates, and ferrous olivine in Allende AOAs resulted from aqueous alteration of the originally unaltered AOAs composed of forsterite, melilite, anorthite, spinel, and Al, Ti-diopside, followed by thermal metamorphism; both processes occurred in an asteroid setting.

2.1.2. AOAs in the Bali-like oxidized CV chondrites

AOAs in the CV_{oxB} chondrites are texturally similar to those in the CV_{oxA} chondrites, but show important mineralogical differences. They consist of forsterite ($Fa_{<2}$; Fig. 1b) and CAIs composed of Al-diopside, anorthite, and minor magnesian

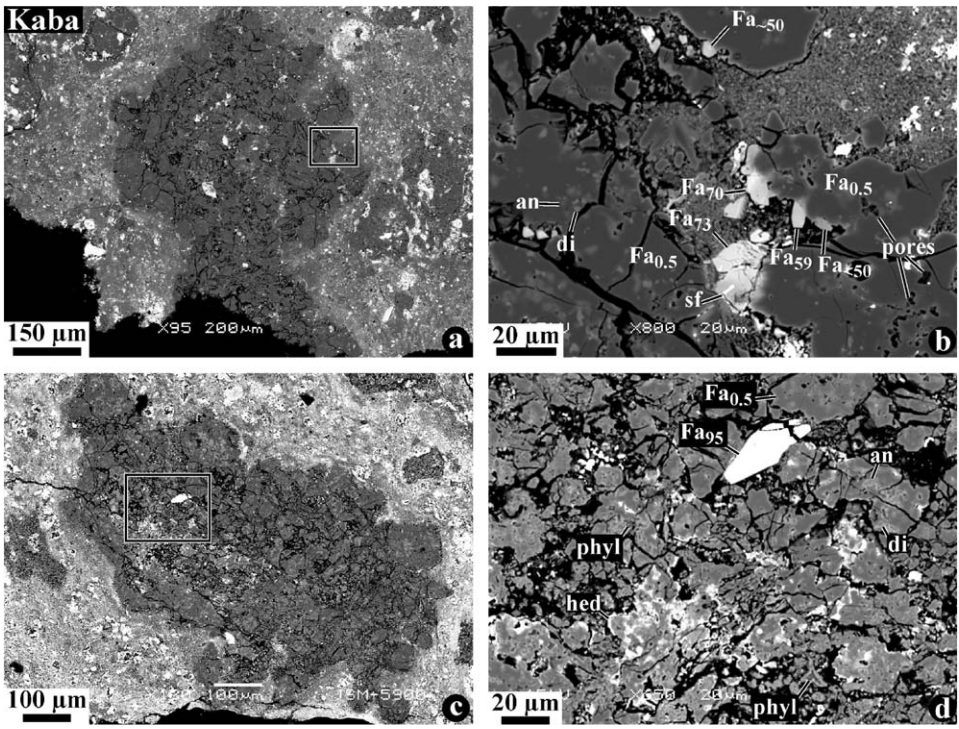


Fig. 4. BSE images of AOAs from the CV_{oxB} chondrite Kaba. AOAs consist largely of forsterite ($Fa_{0.5}$), Al-diopside (di), and anorthite (an). Anorthite is replaced by phyllosilicates (phyl) or leached out leaving behind pores. Forsterite grains are overgrown by euhedral grains of ferrous olivine ($Fa_{50–73}$) and hedenbergitic pyroxenes (hed). Euhedral fayalite grains are also observed inside AOAs, in direct contact with forsterite. Regions outlined in (a) are shown in detail in (b), (c); region outlined in (c) is shown in detail in (d).

spinel (Fig. 4). Anorthite is typically replaced by phyllosilicates or leached out, leaving behind abundant pores (Fig. 4b and d). In contrast to the CV_{oxA} AOAs, nepheline and sodalite are absent. Secondary ferrous olivine of variable composition ($Fa_{\sim 50–95}$) and Ca, Fe-rich pyroxenes of variable composition ($Fs_{10–50}Wo_{45–50}$) growing in pore space and along grain boundaries are commonly observed (Fig. 4). These alteration features are similar to those previously described in CAIs, chondrules, and matrices of the CV_{oxB} Bali, Kaba, and Mokoia (e.g., Keller and Buseck, 1990; Keller et al., 1994; Hua and Buseck, 1995; Krot et al., 1998a, b, 2004b; Choi et al., 2000).

No oxygen isotopic compositions and trace element abundances have yet been reported for AOAs in the CV_{oxB}.

2.1.3. AOAs in the reduced CV chondrites

2.1.3.1. Mineralogy and petrology. AOAs in the reduced CV chondrites are irregularly shaped objects, up to 5 mm in size. They consist of forsteritic olivine ($Fa_{1–10}$; Fig. 1c), Fe, Ni-metal and variable amounts (from <1 to >90 vol%) of CAIs composed of variable amounts of Al-diopside, anorthite, magnesium-rich spinel (~ 1 wt% FeO), and melilite (Figs. 5 and 6). Melilite is replaced either by anorthite or by a fine-grained mixture of spinel and Al-diopside. Secondary nepheline and sodalite replacing anorthite and melilite are generally very minor. Phyllosilicates, fayalite, andradite, and Ca, Fe-rich pyroxenes were not observed. One of the AOAs in Efremovka contains low-Ca pyroxene ($Fs_{1.9}Wo_{1.4}$) that replaces forsterite ($Fa_{0.8}$) in the peripheral portion of the AOA (Fig. 7). Although AOAs show no clear evidence for melting and contain abundant pores, some of the CAIs inside AOAs have compact textures and rounded outlines, suggesting an igneous origin.

2.1.3.2. Trace elements. Russell et al. (2003) reported trace element abundances in six AOAs in Efremovka analyzed by LA-ICP-MS. Most AOAs have unfractionated REE patterns and present at levels of $\sim$10CI; one AOA (#4) has a Type VI pattern, characterized by positive enrichments in Eu and Yb (Fig. 2b).

2.1.3.3. Oxygen isotopic compositions. Oxygen isotopic compositions of AOAs in the reduced CV chondrites show complex patterns (Fagan et al., 2004; Fig. 3b–d). Forsteritic olivines are always ^{16}O-enriched ($\Delta^{17}O \sim -20‰$). Ferrous olivine rims around forsterite grains in Efremovka AOAs are ^{16}O-depleted (Fig. 3b). The depletion is correlated with the OH-signal collected during the analyses—indicative of hydrated mineral(s). Two AOAs from Leoville and one from Vigarano, showing minimal Fe-alkali metasomatic alteration, have mineral-dependent O-isotopic systematics: forsterite is ^{16}O-rich, anorthite is ^{16}O-poor, and Al-diopside shows a range of intermediate compositions (Fig. 3c and d). Another Vigarano AOA, characterized by extensive Fe-alkali metasomatic alteration, largely preserved the original ^{16}O-rich composition in olivine, but has an ^{16}O-poor anorthite.

Based on these observations and oxygen isotope diffusion modeling, Fagan et al. (2004) concluded that alteration of the Efremovka and Vigarano AOAs occurred in the presence of aqueous solutions, whereas the distribution of O-isotopic

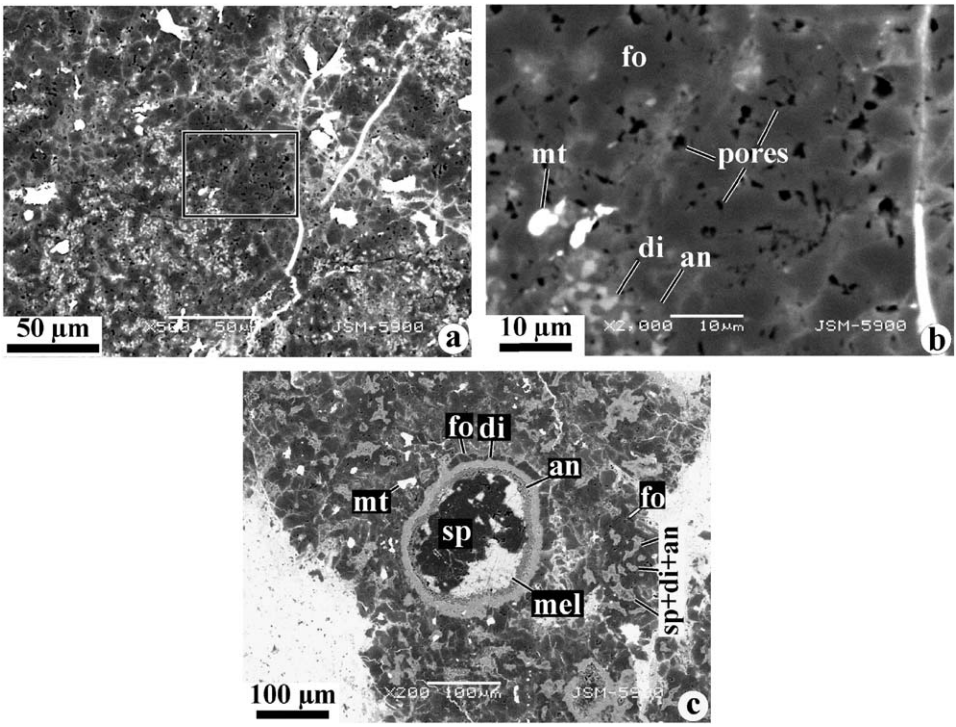


Fig. 5. BSE images of two AOAs in the reduced CV chondrite Efremovka shown on a cover page. AOAs consist of fine-grained forsteritic olivines (fo), Fe, Ni-metal (mt), and fine-grained CAIs largely composed of Al-diopside (di), anorthite (an), and minor spinel (sp). (a, b) AOA #1 is very porous and contains CAIs that show no mineralogical zoning. Region outlined in "a" is shown in detail in "b". (c) AOA #2 is rather compact and contains mineralogically-zoned fine-grained CAIs which have a spinel core surrounded by the layers of anorthite, Al-diopside and forsterite. It also contains several coarse-grained, rounded CAIs composed of spinel and melilite and surrounded by the layers of anorthite, Al-diopside and forsterite; anorthite replaces melilite.

compositions in the Leoville AOAs could have resulted from oxygen isotope exchange at temperature of 1100–1300°C during transient heating events.

2.1.4. Forsterite-rich accretionary rims in the reduced and Allende-like oxidized CV chondrites

2.1.4.1. Mineralogy and petrology. Coarse-grained, accretionary rims (different from fine-grained, matrix-like rims) were first described around several CAIs from the oxidized CV chondrite Allende by MacPherson et al. (1985), who distinguished them from coarse-grained, igneous rims around chondrules (Rubin, 1984) and Wark-Lovering rims (WLR) around CAIs (Wark and Lovering, 1977). The accretionary rims in Allende are characterized by multilayered structures, with layers differing from one another in texture, mineralogy and mineral chemistry. As

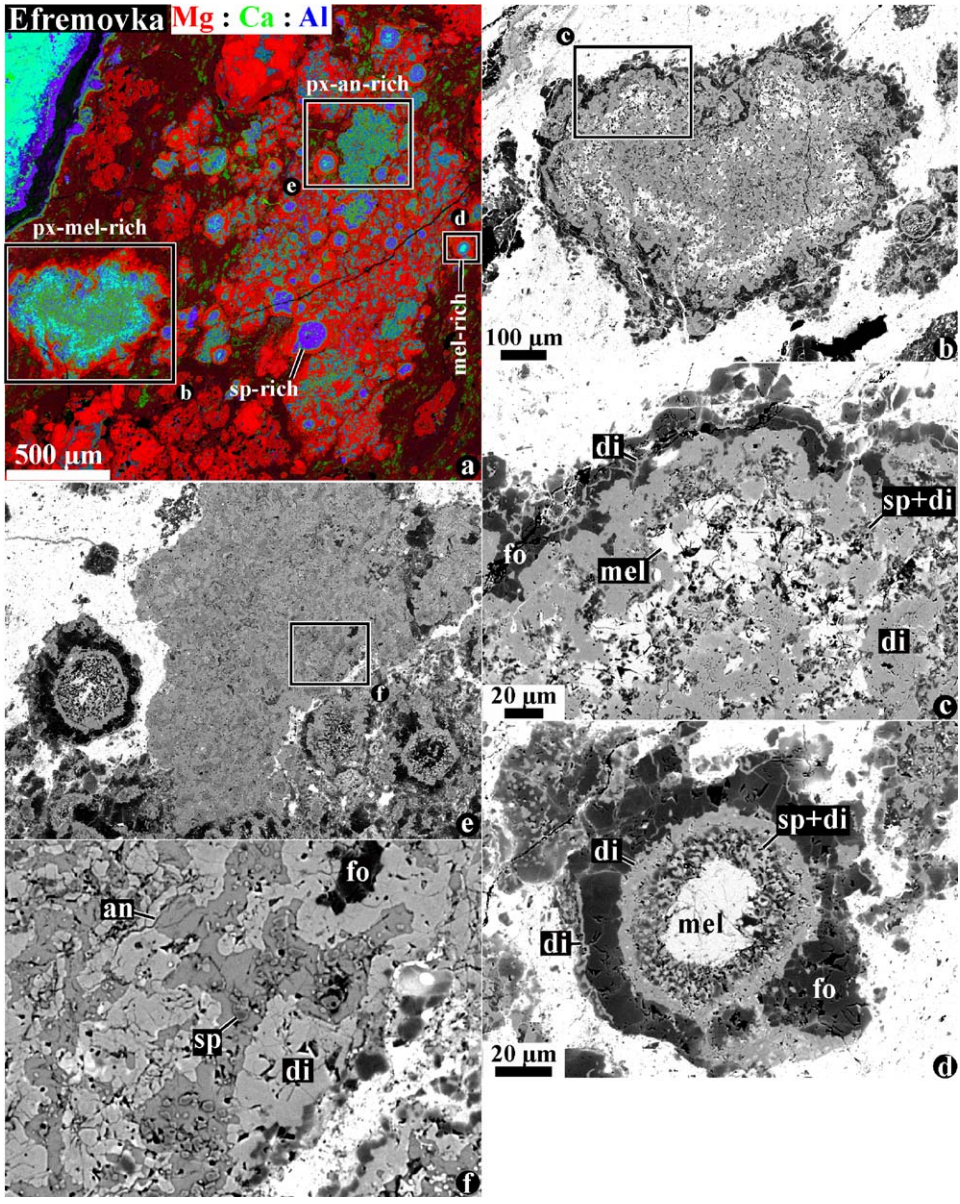


Fig. 6. Combined elemental map in Mg (red), Ca (green), and Al$K\alpha$ (blue) X-rays (a), and BSE images (b–f) of AOA in the reduced CV chondrite Efremovka. It consists of fine-grained, forsteritic olivines (fo), and abundant, rounded and irregularly shaped CAIs composed of spinel (sp), Al-diopside (di), $\pm$anorthite (an), and $\pm$melilite (mel). Melilite is typically replaced by a fine-grained mixture of spinel and Al-diopside. There are large variations in modal mineralogy of the CAIs. Although the entire AOA shows no clear evidence for being melted, compact and rounded CAIs may have experienced melting. Regions outlined in (b) and (e) are shown in detail in (c) and (e), respectively.

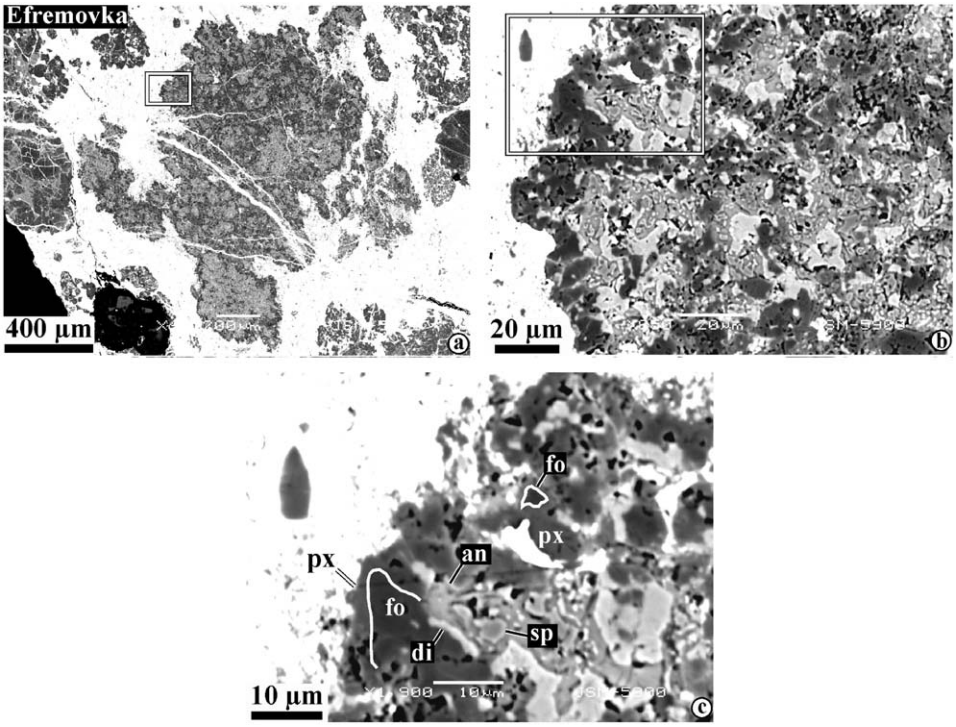


Fig. 7. BSE images of AOA with low-Ca pyroxene in the reduced CV chondrite Efremovka. AOA consists of forsteritic olivine (fo), Fe, Ni-metal (mt), Al-diopside (di), anorthite (an), spinel (sp), and low-Ca pyroxene (px). Spinel is corroded by anorthite. Low-Ca pyroxene occurs in the outermost portion of AOA and replaces forsterite. Region outlined in (a) and (b) are shown in detail in (b) and (c), respectively.

defined by MacPherson et al. (1985), the innermost layer consists of either high-Ca pyroxene needles + olivine + clumps of hedenbergite and andradite (IA) or olivine "doughnuts" (IB) (i.e., crystals with central cavities). The next layers outward (II, III) contain olivine plates and laths. The final layer (IV) separating accretionary rims from the Allende matrix occurs as clumps of andradite + hedenbergite surrounded by salitic pyroxene needles. Nepheline and Fe, Ni-sulfides are common constituents in all layers. Based on the observed disequilibrium mineral assemblages, abundant euhedral crystals with pore space between them, and rim thicknesses controlled by the underlying topography of their host inclusions, MacPherson et al. (1985) concluded that the layered accretionary rims in Allende are aggregates of gas–solid condensates which reflect significant fluctuations in physicochemical conditions in the solar nebula and grain/gas separation processes.

In the reduced CV chondrites Efremovka, Leoville and Vigarano, accretionary rims around CAIs show no layering; they are mineralogically similar to AOAs in their host meteorites (Krot et al., 2001b, 2002b, 2004c). These rims consist of

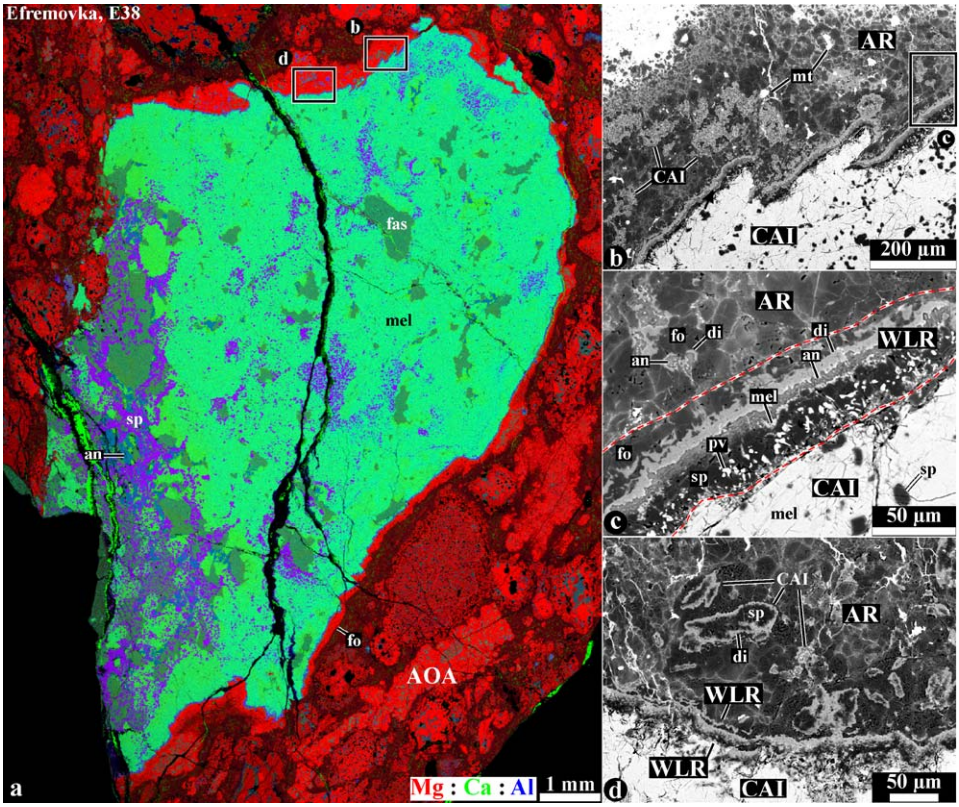


Fig. 8. (a) Combined elemental map in Mg (red), Ca (green) and Al *Kα* (blue) X-rays of a type B CAI E38 from the reduced CV chondrite Efremovka; (b–d) BSE images from regions marked in elemental map. This CAI consists of melilite (mel), Al, Ti-diopside (fas), spinel (sp), and anorthite (an) and is surrounded by a multilayered, WLR composed of spinel, perovskite (pv), anorthite, Al-diopside, and forsterite, and a thick outer forsterite-rich, accretionary rim (AR; red in (a)). The accretionary rim consists of forsterite (ol), Fe, Ni-metal (mt), and CAIs composed of spinel, Al-diopside, and anorthite. There are significant variations in modal mineralogy of the CAIs in the accretionary rim (from Scott and Krot, 2003). Regions outlined in (a) are shown in detail in (b) and (d); region outlined in (b) is shown in detail in (c).

coarse-grained (20-40 µm), anhedral forsterite (Fa_{1-8}), Fe, Ni-metal nodules, and fine-grained CAIs composed of Al-diopside, anorthite, and spinel, ±forsterite; no chondrule-like materials were found in the rims. The rims surround different types of CAIs (compact and fluffy Type A, Type B, and fine-grained, spinel-rich) and occur outside WLRs (Fig. 8).

Based on these observations and a thermodynamic analysis, Krot et al. (2001b, 2002b, 2004c) concluded that (1) forsterite-rich, accretionary rims formed by aggregation of high-temperature condensates around CAIs at or below the forsterite

condensation temperature. (2) The aggregation of rims postdated high-temperature events experienced by the CAIs, such as melting and formation of WLRs, and occurred in CAI-forming region(s). (3) The absence of andradite, wollastonite, and hedenbergite from the Efremovka rims and their presence in the Allende rims suggest that these minerals are secondary and resulted from late-stage metasomatic alteration under oxidizing conditions.

2.1.4.2. Oxygen isotopic compositions. Hiyagon (1998) reported oxygen isotope compositions of minerals in accretionary rims around two Type A CAIs from Allende. Olivines in both accretionary rims are characterized by ^{16}O-rich isotopic compositions ($\delta^{18}O = -28‰$, $\delta^{17}O = -30‰$), whereas wollastonite, andradite and hedenbergite show nearly normal oxygen isotopic compositions ($\delta^{18}O$ from $+2‰$ to $+10‰$, $\delta^{17}O$ from $-3‰$ to $+4‰$). Hiyagon (1998) concluded that accretionary rims originated in the CAI-forming regions, where they acquired their anomalous ^{16}O-rich isotope compositions, but had addressed neither the nature of ^{16}O-enrichment nor the origin of ^{16}O-poor minerals in the rims.

McKeegan et al. (1998) and Krot et al. (2002b) reported oxygen isotopic compositions of two Type A CAIs (E104 and 1623-3) surrounded by the Wark-Lovering and forsterite-rich, accretionary rims in the reduced CV chondrites Efremovka and Vigarano. The oxygen isotope data for E104 show a bimodal distribution (Fig. 9a). Spinel and pyroxene in both the CAI and its WLR, as well as coarse-grained forsterite in the accretionary rim, have nearly identical ^{16}O-rich compositions; melilite is ^{16}O-poor and plots near the terrestrial fractionation line.

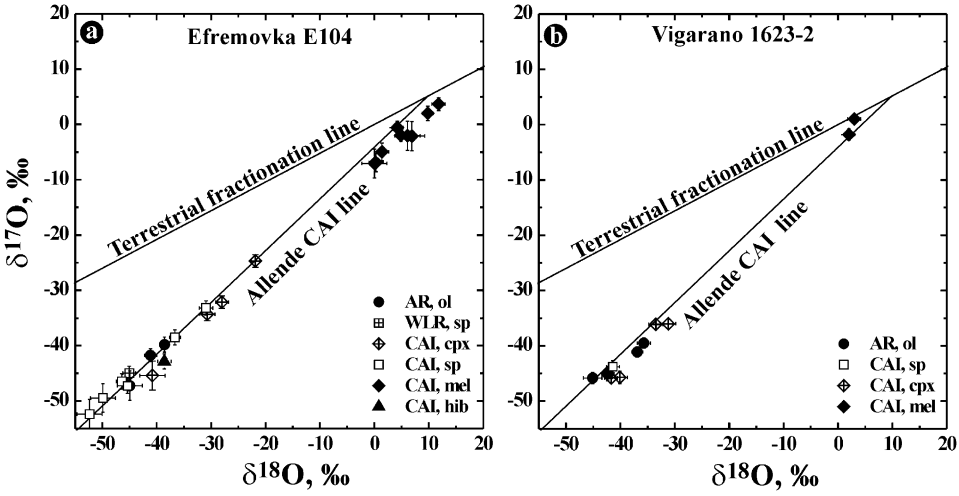


Fig. 9. Oxygen isotopic compositions (errors are 1σ) of individual minerals in the Efremovka Type A CAI E104 (a) and Vigarano Type A CAI 1623-2 (b) and their forsterite-rich, accretionary rims showing that both formed in an ^{16}O-rich reservoir (from Krot et al., 2002b). cpx—Al-diopside, hib—hibonite, mel—melilite, ol—forsteritic olivine, and sp—spinel.

Small variations in oxygen isotope compositions of pyroxenes result from overlap of ion probe spots with neighboring melilite and anorthite. Similar variations in the composition of fine-grained forsterite in the accretionary rims probably reflect beam overlap onto isotopically heavy, secondary ferrous olivine rims along forsterite grain boundaries.

The oxygen isotope data for the Vigarano CAI (Fig. 9b) scatter more uniformly along the Allende CAI line than that for E104: spinel and hibonite are ^{16}O-rich ($\delta^{17,18}O \sim -40‰$ to $-50‰$), and melilite plots near the ^{16}O-depleted end of the mixing line. Spinel in the WLR and forsterite in the accretionary rim are indistinguishable from interior spinel grains. The pyroxene layer shows a range in oxygen isotope composition ($\delta^{17,18}O \sim -20‰$ to $-40‰$).

Based on these observations, Krot et al. (2002b) concluded that CAIs surrounded by forsterite-rich accretionary rims formed in the presence of ^{16}O-rich nebular gas. The observed differences in oxygen isotopic compositions between forsterite and secondary Ca, Fe-rich minerals in the Allende accretionary rims (Hiyagon, 1998) suggest that the secondary minerals formed in the presence of a fluid having ^{16}O-poor oxygen isotopic composition. No trace element data for forsterite-rich accretionary rims have yet been reported.

2.2. AOAs in CO chondrites

2.2.1. Mineralogy and petrology

CO chondrites are known to have experienced Fe-alkali metasomatic alteration and thermal metamorphism to varying degrees and are divided into petrologic subtypes from 3.0 to 3.9. The alteration affected CAIs, chondrules and matrices of CO chondrites and resulted in formation of nepheline, sodalite, ferrous olivine, magnetite, Fe, Ni-carbides and sulfides (e.g., Russell et al., 1998; Itoh and Tomeoka, 2003a). There is a correlation between the degree of alteration and thermal metamorphism experienced by CO chondrites, suggesting that alteration most likely occurred in an asteroid setting during fluid-assisted thermal metamorphism.

The mineralogy and petrology of AOAs in CO chondrites have recently been characterized by Rubin (1998) and Chizmadia et al. (2002). In the least metamorphosed CO3.0 chondrites ALHA77307 and Y-81020, most AOAs consist of forsterite ($Fa_{<2}$; Fig. 1e), Fe, Ni-metal, and CAIs composed of Al-diopside, anorthite, and $\pm$spinel. Spinel grains, which are nearly pure $MgAl_2O_4$, are either surrounded by anorthite (Fig. 10a and b) or by fine-grained symplectitic intergrowths of spinel and diopside, which most likely replace melilite (Fig. 10c); no remnants of melilite have been reported, however. Spinel and olivine in AOAs in CO chondrites of petrologic subtype 3.2–3.8 show enrichment in FeO (Fig. 10b–d); anorthite is replaced by nepheline and sodalite (Fig. 10d–f). In petrologic subtype 3.2 narrow veins of fayalitic olivine form along forsterite grain boundaries. With increasing degree of thermal metamorphism, these veins thicken to form zones of ferrous olivine in the AOA peripheries (Figs. 1g and 10d). In subtype 3.8, no forsterite remains and olivine has a composition in the range of $Fa_{64–67}$ (Figs. 1h and 10e). Chizmadia et al. (2002) concluded that mineral changes in AOAs in CO

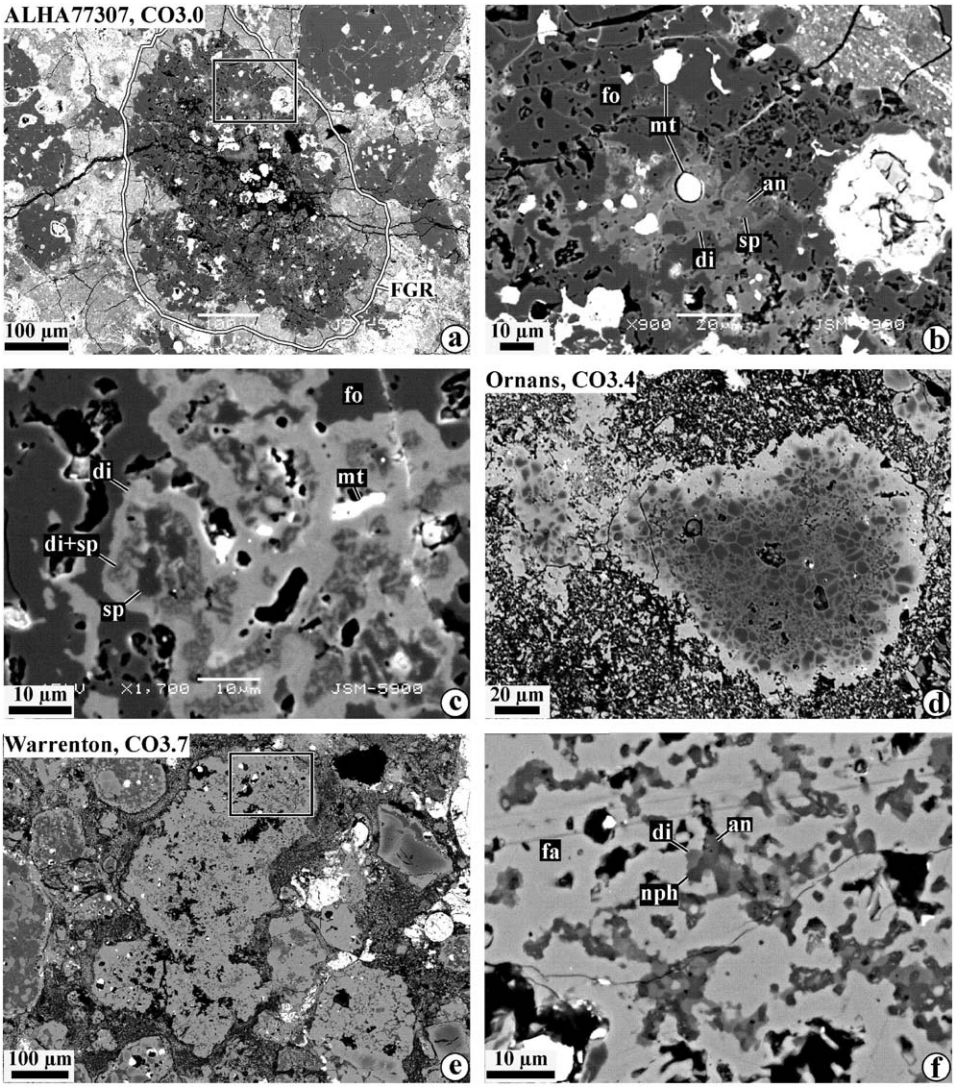


Fig. 10. BSE images of AOAs in CO chondrites of different petrologic subtypes: (a–c) ALHA77307 (3.0), (d) Ornans (3.4) and (e, f) Warrenton (3.7). AOAs in ALHA77307 consist of forsterite ($Fa_{<2}$; fo), Fe, Ni-metal (mt) and CAIs composed of Al-diopside (di), anorthite (an) and spinel (sp). Spinel is corroded by anorthite. Symplectitic intergrowths of diopside and spinel in (c) must have resulted from replacement of melilite. AOAs are surrounded by fine-grained rims (outlined in (a)). AOA in Ornans shows enrichment in FeO along forsterite grain boundaries and at periphery. Olivine grains (fa) in AOA in Warrenton are uniformly FeO-enriched ($Fa_{63–67}$); anorthite is largely replaced by nepheline (nph).

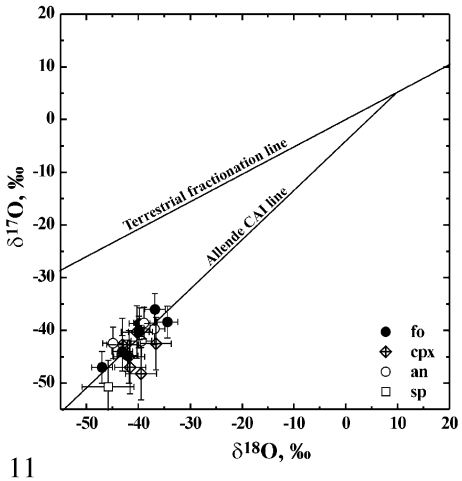
chondrites of low petrologic subtype required aqueous solutions, whereas those in subtypes >3.3 largely reflect diffusive exchange within and between mineral grains without the aid of fluids.

2.2.2. Oxygen isotopic compositions

Oxygen isotopic compositions of AOAs in CO chondrites of different petrologic subtypes [ALHA77307, Y-81020 (3.0), Kainsaz (3.1), Y-82050 (3.2), and Y-791717 (3.3)] have been reported by Hiyagon and Hashimoto (1999b, c), Hiyagon (2000), and Itoh et al. (2002). Forsterite, spinel, Al-diopside and anorthite in AOAs in ALH77307 and Y-81020 are uniformly ^{16}O-enriched ($\delta^{17,18}O \sim -40‰$ to $-50‰$; Fig. 11). Hiyagon and Hashimoto (1999b) also discovered ^{16}O-rich ($\delta^{17,18}O \sim -40‰$) enstatite associated with forsterite in an "enstatite-rich mantle" of an AOA in ALHA77307.

Olivines in AOAs in Y-82050 and Y-791717 show a range in oxygen isotopic compositions ($\delta^{17,18}O \sim -15‰$ to $-50‰$; Figs. 1 and 2 in Hiyagon and Hashimoto, 1999b), but no obvious correlation between fayalite content and oxygen isotopic compositions (Fig. 2 in Hiyagon and Hashimoto, 1999c); spinel and Al-diopside are ^{16}O-rich. No anorthite, melilite, or secondary nepheline have been reported in AOAs in metamorphosed CO chondrites.

Two relict AOAs found in ferromagnesian chondrules in Y-81020 and Kainsaz (3.2) retained their original ^{16}O-rich ($\delta^{17,18}O \sim -40‰$) isotopic composition;



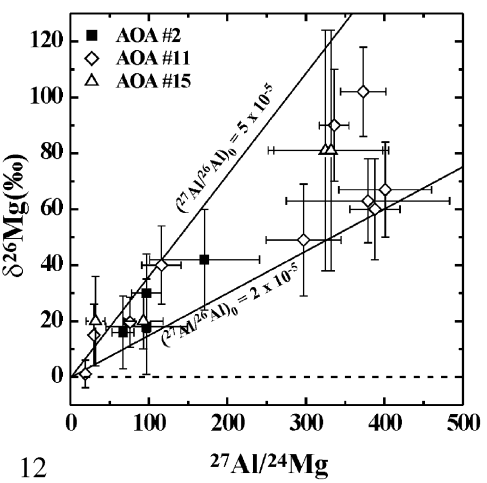


Fig. 11. Oxygen isotopic compositions of individual minerals in AOAs in the CO3.0 chondrite Y-81020 (from Itoh et al., 2003). an—anorthite, fo—forsterite, di—Al-diopside, and sp—spinel.

Fig. 12. Al-Mg systematics of AOAs in the Y-81020 CO3.0 chondrite. The AOAs show ^{26}Mg* corresponding to the initial $(^{26}Al/^{27}Al)_0$ ratios between 2×10^{-5} and 5×10^{-5} (from Itoh et al., 2002).

chondrule phenocrysts (olivine and pigeonite) are ^{16}O-depleted ($\delta^{17,18}O \sim 0‰$) (Itoh et al., 2002; Fig. 11).

2.2.3. Al–Mg systematics

Three AOAs in Y-81020 were studied for Al–Mg systematics (Itoh et al., 2002). These showed excess of ^{26}Mg (^{26}Mg*) corresponding to the initial ^{26}Al/^{27}Al ratios of $(2.7 \pm 0.7) \times 10^{-5}$ (AOA ♯11) $(2.9 \pm 1.5) \times 10^{-5}$ (AOA ♯2) and $(3.2 \pm 1.5) \times 10^{-5}$ (AOA ♯15) (Fig. 12). Because the $(^{26}Al/^{27}Al)_0$ in most CAIs is $\sim 4–5 \times 10^{-5}$ (e.g., MacPherson et al., 1995), Itoh et al. (2002) suggested that either AOAs formed 0.1–0.5 Ma after CAIs or that ^{26}Al was heterogeneously distributed in the CAI-forming region. No ^{26}Mg* was detected in the AOA-bearing chondrule (Itoh et al., 2002). No trace element data for CO AOAs have yet been reported.

2.3. AOAs in CM chondrites

2.3.1. Mineralogy and petrology

AOAs are the dominant type of refractory inclusions in all CM chondrites, but have been studied in detail only in Murchison (e.g., MacPherson et al., 1988). They consist of forsterite ($Fa_{<2}$; Fig. 1d) and a refractory component (individual CAIs and fine-grained minerals interspersed with forsterite grains) composed of spinel, Al-diopside and anorthite or its alteration products, phyllosilicates or carbonates (Fig. 13a, b and d). In some cases, most of the refractory minerals have been leached out, leaving behind abundant pores (Fig. 13c). One anomalous AOA (Fig. 13e and f) is a very compact object (no pores were observed) that shows large compositional variations of olivine: Fa and MnO contents increase (3–7 mol% and 0.4–0.9 wt%, respectively), whereas CaO contents decrease (0.4–0.2 wt%) from core to rim of the AOA (Fig. 14). The presence of refractory inclusions composed of spinel surrounded by Al-diopside distinguishes this AOA from ferromagnesian chondrules. Another compact AOA contains low-Ca pyroxene replacing forsterite along the AOA periphery; low-Ca pyroxene also forms haloes around opaque nodules inside AOA (Fig. 15). The AOA may have experienced a small degree of melting, indicated by the presence of euhedral grains of Al-diopside in anorthite. Like other coarse-grained components in CM chondrites, AOAs in Murchison are commonly surrounded by fine-grained matrix-like rims (Fig. 13b).

2.3.2. Oxygen isotopic compositions

Spinel, Al-diopside, and forsterite in Murchison AOAs, including a compact AOA with compositionally zoned olivine grains (Fig. 13e and f), are ^{16}O-enriched ($\Delta^{17}O < -20‰$) (Hiyagon and Hashimoto, 1999a; Krot et al., 2004d; Fig. 16). Low-Ca pyroxene replacing forsterite in the outermost portion of the AOA shown in Fig. 15 is ^{16}O-depleted. No trace element measurements in CM AOAs have yet been reported.

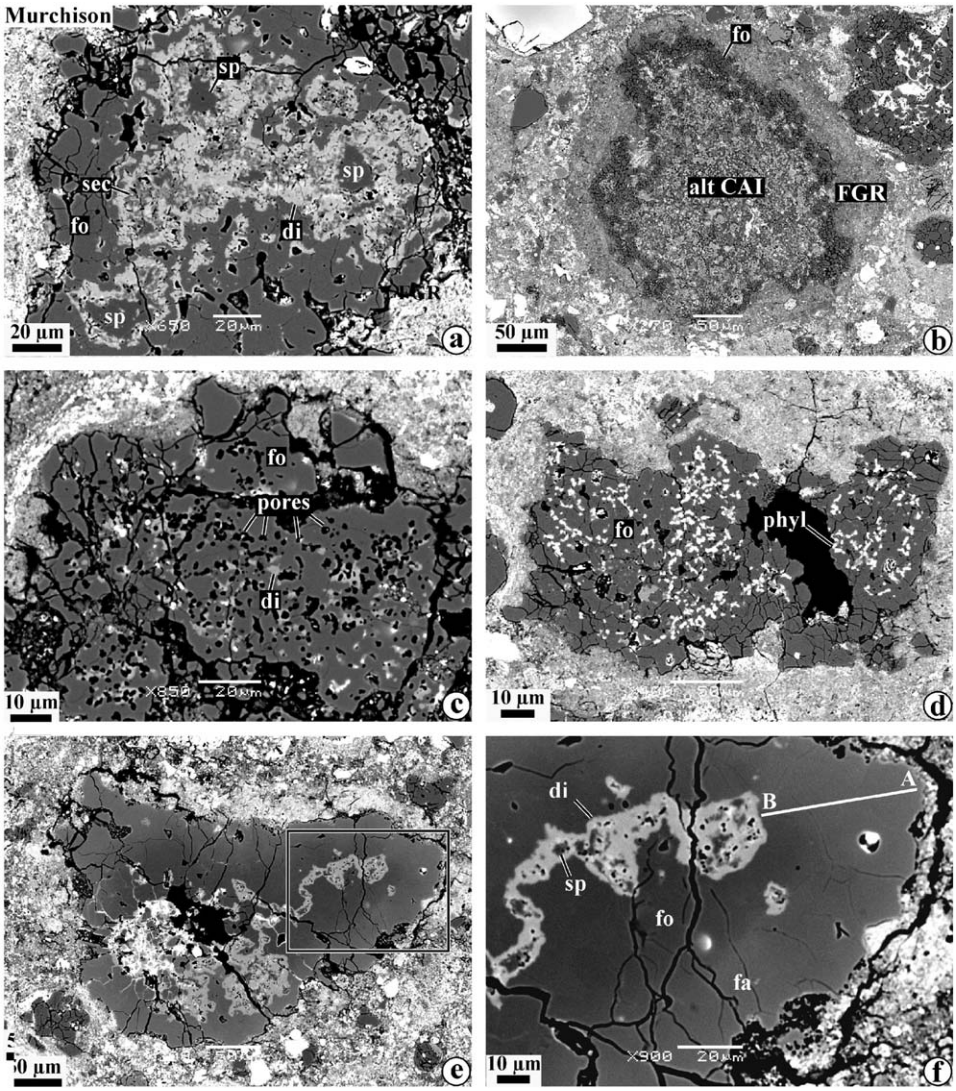


Fig. 13. (a–f) BSE images of AOAs in the CM carbonaceous chondrite Murchison. The AOAs consist of forsterite (fo) and variable amounts of altered CAIs composed of spinel (sp), secondary phases (sec), and Al-diopside (di). The secondary phases, probably phyllosilicates, replace anorthite or melilite. In some AOAs, the CAI minerals are leached out leaving behind pores (see (c)). AOAs are commonly surrounded by fine-grained, accretionary rims (FGR). (e,f) Compact AOA showing large compositional variations in olivine compositions. AB indicates compositional profile shown in Fig. 14.

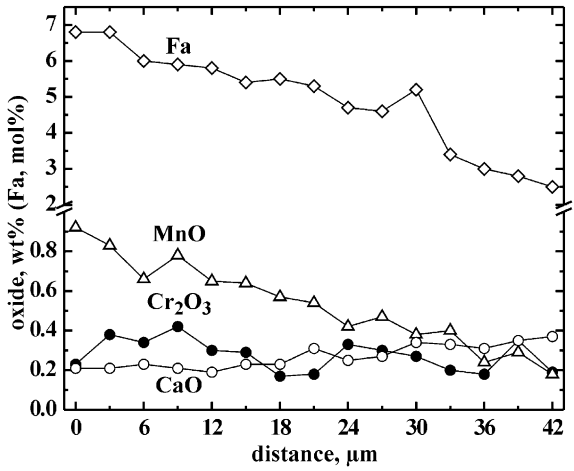


Fig. 14. Compositional profile (AB) across olivine in AOA from Murchison shown in Fig. 10e and f.

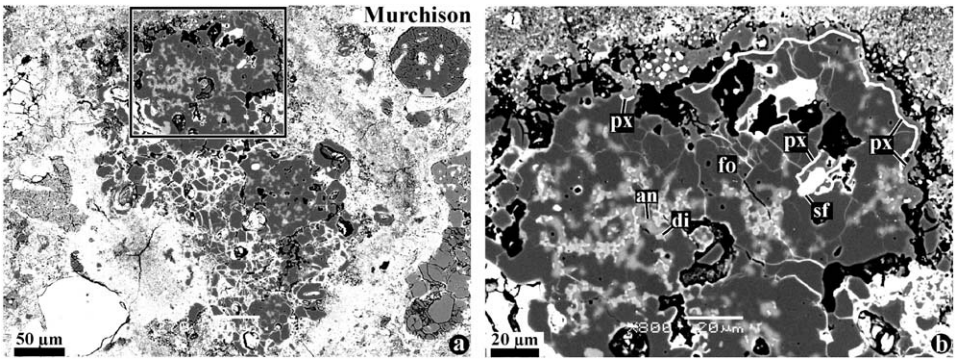


Fig. 15. BSE images of AOA with low-Ca pyroxene in Murchison. The AOA consists of forsterite (fo), anorthite (an), Al-diopside (di), Fe, Ni-sulfides (sf), and low-Ca pyroxene (px). Al-diopside occurs as subhedral grains in anorthite, suggesting crystallization from melt. Low-Ca pyroxene (outlined in (b)) replaces forsterite in the outermost portion of AOA; it also forms a layer around sulfide nodule. Region outlined in (a) is shown in detail in (b).

2.4. AOAs in CR chondrites

2.4.1. Mineralogy and petrology

The mineralogy and petrology of AOAs in CR chondrites have recently been characterized by Aléon et al. (2002), Weisberg et al. (2003), and Krot et al. (2003a,b, 2004d). The CR AOAs consist of forsterite ($Fa_{<2}$; Fig. 1j), Fe, Ni-metal, and CAIs composed of Al-diopside, anorthite, and minor spinel, which is corroded by

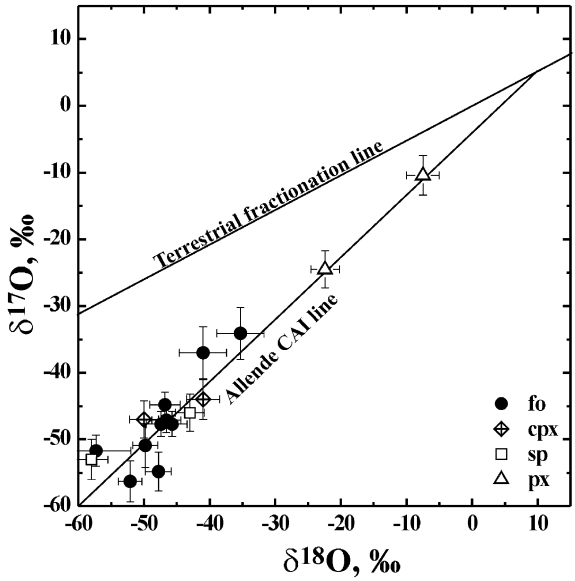


Fig. 16. Oxygen isotopic compositions (errors are 1σ) of individual minerals in AOAs in Murchison (data from Hiyagon and Hashimoto (1999a–c) and Krot et al. (2004d). cpx—Al-diopside, fo—forsterite, px—low-Ca pyroxene, and sp—spinel.

anorthite. Melilite is very rare and replaced by a fine-grained mixture of spinel, Al-diopside, and anorthite (Fig. 17a–d). Aluminum-diopside in contact with this reaction zone often shows enrichment in Al_2O_3 (Fig. 17c). Some AOAs are exceptionally rich in Fe, Ni-metal (Fig. 17e and f). Forsterites in outer portions of AOAs are commonly enriched in MnO (up to 1.2 wt%) relative to those from their cores (Weisberg et al., 2003; Krot et al., 2004e).

About 10% of CR AOAs contain low-Ca pyroxene replacing forsterite (Krot et al., 2004e). There are several textural occurrences of low-Ca pyroxene in AOAs: (i) veinlets along forsterite grain boundaries and thin discontinuous layers around forsterite grains in AOA peripheries; (ii) haloes around Fe, Ni-metal grains, and (iii) thick continuous layers with abundant tiny inclusions of Fe, Ni-metal nodules around AOAs (Figs. 18 and 19).

AOAs in most CR chondrites studied show no evidence for alteration. However, Renazzo and Al Rais experienced extensive aqueous alteration resulting in replacement of anorthite or melilite in AOAs by phyllosilicates (Fig. 17e and f).

2.4.2. Oxygen isotopic compositions

Oxygen isotopic compositions of seven CR AOAs and a CB CAI reported by Aléon et al. (2002) and Krot et al. (2004d) are plotted in Fig. 20. Forsterite, anorthite, Al-diopside, and spinel in these AOAs are uniformly ^{16}O-rich ($\Delta^{17}O < -20‰$). Low-Ca pyroxenes replacing forsterite along grain boundaries and around Fe, Ni-metal nodules (Fig. 17a–e) are ^{16}O-enriched ($\Delta^{17}O < -20‰$).

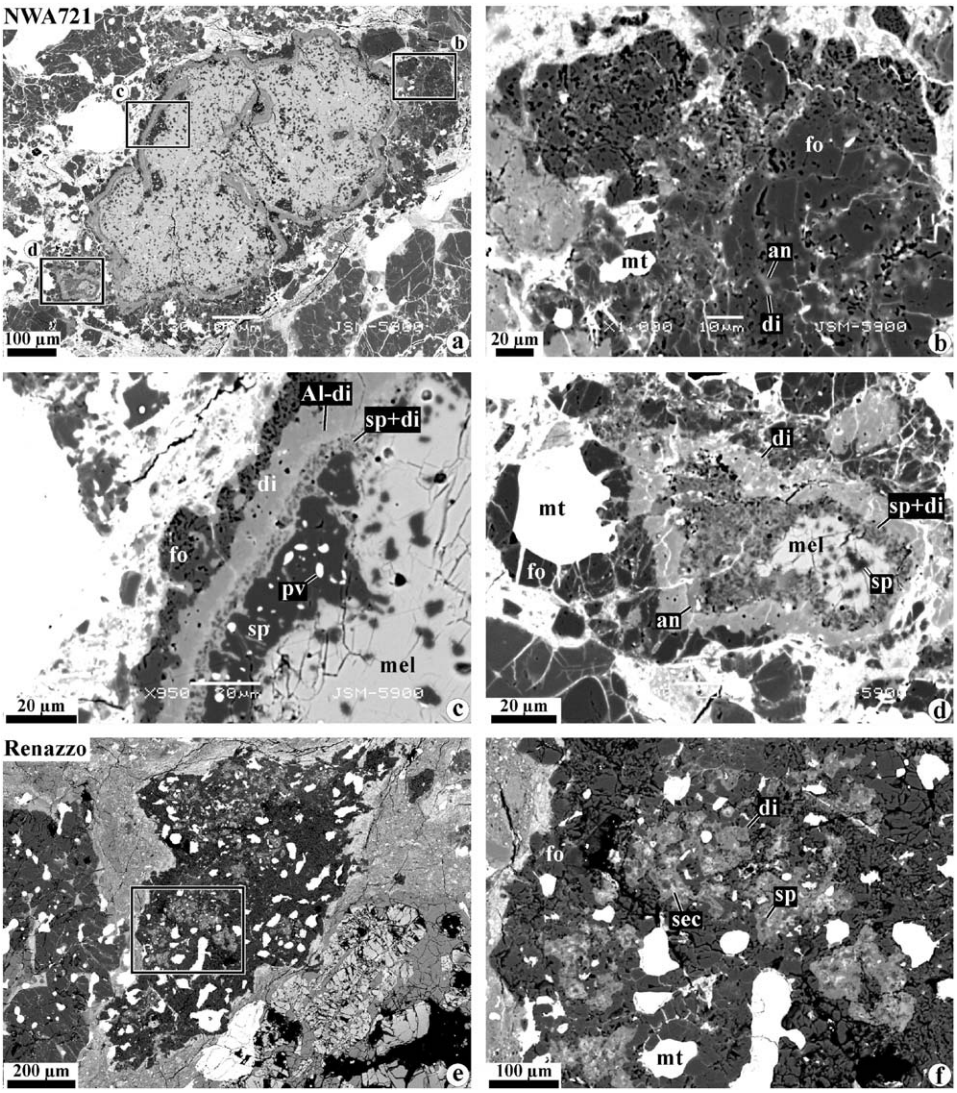


Fig. 17. BSE images of AOAs in the CR carbonaceous chondrites NWA 721, Renazzo, and Gao-Guenie (b). (a–d) The NWA 721 AOA contains a coarse-grained, compact Type A CAI composed of melilite (mel), spinel (sp) and perovskite (pv). The CAI is surrounded by a rim of diopside (di). Melilite near the rim is replaced by a fine-grained mixture of spinel and diopside; Al_2O_3 content in the rim diopside sharply increases towards this alteration zone. CAI is surrounded by a porous aggregate of forsterite with tiny inclusions of anorthite and Al-diopside, and Fe, Ni-metal. (e,f) The Renazzo AOA consists of forsterite, abundant Fe, Ni-metal nodules, and CAIs composed of Al-diopside, spinel and secondary phases (phyllosilicates?), which probably replace either anorthite or melilite.

Low-Ca pyroxenes occurring as thick rims around AOAs (Figs. 18f and 19) have ^{16}O-poor compositions ($\Delta^{17}O > -5‰$) (Fig. 20).

2.5. AOAs in CH chondrites

AOAs in CH chondrites are small ($\sim$150–180 μm in apparent diameter) and relatively common: 15 AOAs were identified in two thin sections of NWA 739 and NWA 770. AOAs typically consist of forsterite ($Fa_{<2}$; Fig. 1k), Fe, Ni-metal, and CAIs composed of Al-diopside, anorthite and rare spinel grains (Fig. 21a–d). Spinel appears to be corroded by anorthite (Fig. 21c and d). One AOA contains several compact CAIs composed of melilite, spinel, and perovskite (Fig. 21e and f). The CAIs are surrounded by thin rims of Al-diopside. Melilite shows only incipient replacement by anorthite. Micron-size rims of low-Ca pyroxene occur along forsterite grain boundaries; low-Ca pyroxene replaces forsterite.

No oxygen isotopic compositions and trace element abundances have yet been reported for AOAs in CH chondrites.

2.6. AOAs in CB chondrites

No AOAs have been observed in the CB_a chondrites Gujba, Bencubbin, and Weatherford (Weisberg et al., 2001; Krot et al., 2001c) and only one AOA was found in the CB_b chondrite Hammadah al Hamra 237. The AOA consists of $\sim$40 vol% of forsteritic olivine (Fa_1) and Fe, Ni-metal, and $\sim$60 vol% of CAIs composed of Al-diopside, anorthite and spinel (Fig. 22). The CAIs have ^{16}O-rich isotopic compositions ($\Delta^{17}O < -20‰$; Fig. 20); no oxygen isotope compositions have been reported for forsterite (Krot et al., 2001c).

2.7. AOAs in the ungrouped carbonaceous chondrite Acfer 094

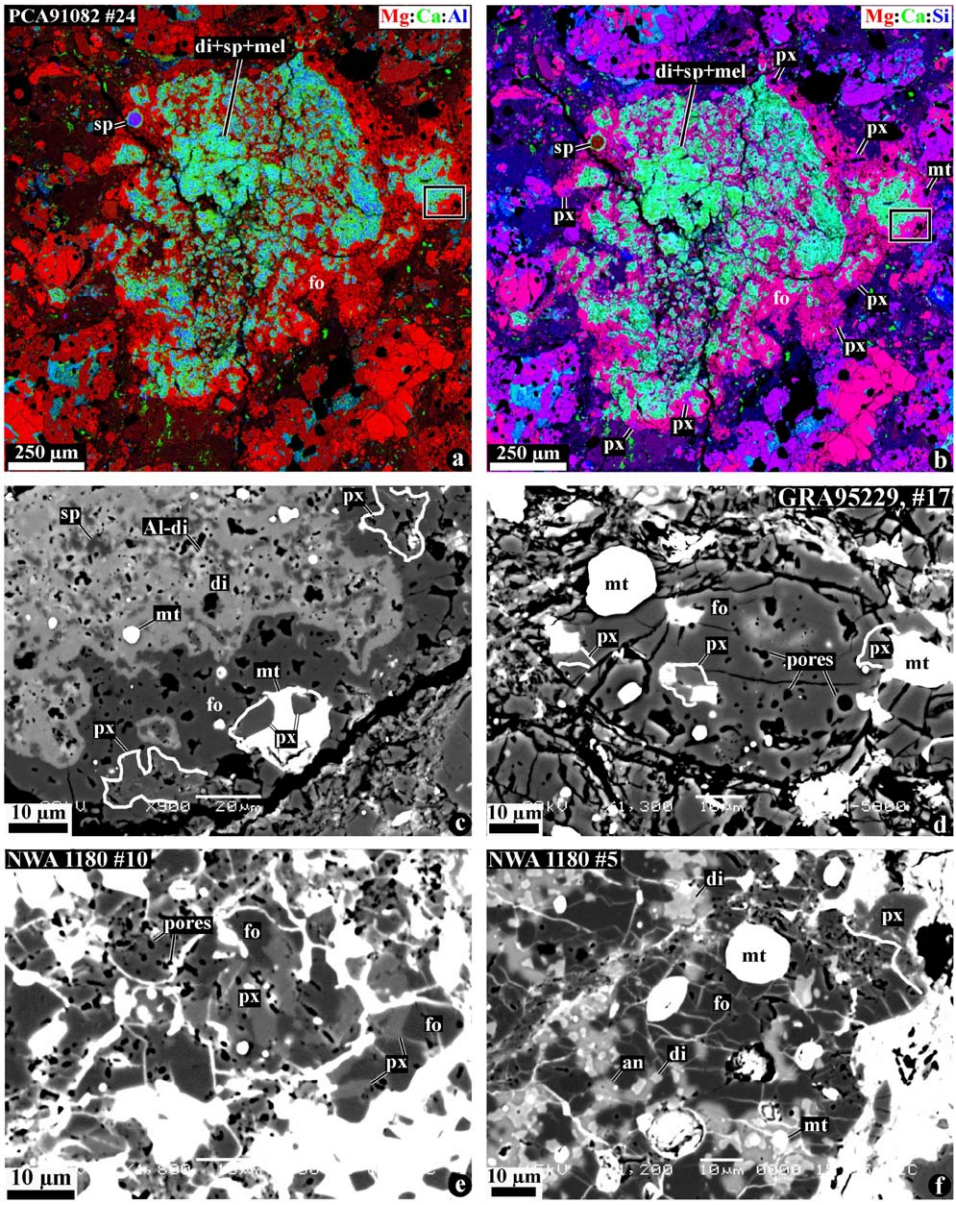
2.7.1. Mineralogy and petrology

Acfer 094 is an ungrouped type 3 carbonaceous chondrite breccia with mineralogical, petrological, nitrogen and oxygen isotopic affinities to the CM and CO groups (Newton et al., 1995; Greshake, 1997). It shows no evidence for thermal metamorphism or alteration, has one of the highest abundances of presolar SiC and diamonds, and amorphous silicates in the matrix, and is considered to be one of the most pristine carbonaceous chondrites in our collections (Greshake, 1997).

AOAs in Acfer 094 consist of forsteritic olivine ($Fa_{<2}$; Fig. 1k), Fe, Ni-metal, and CAIs composed of anorthite, Al-diopside, spinel, and exceptionally rare melilite (Krot et al., 2004a). There are large variations in both the modal mineralogy of the CAIs and the CAI/forsterite ratios. Melilite is replaced by a symplectitic intergrowth of spinel and Al-diopside (Fig. 23a and b). Spinel grains are anhedral and corroded by anorthite. About 5% of AOAs contain variable amounts of low-Ca pyroxene replacing forsterite along grains boundaries in the AOA peripheries and around Fe, Ni-metal nodules (Fig. 23c–f). No other secondary phases have been observed.

2.7.2. Oxygen isotopic compositions

Krot et al. (2004d) measured oxygen isotopic compositions of forsterite and low-Ca pyroxene in the AOAs shown in Fig. 23c–f; both minerals are ^{16}O-enriched ($\Delta^{17}O < -20‰$). No trace element abundances have yet been reported in Acfer 094 AOAs.



2.8. AOAs in the ungrouped carbonaceous chondrite adelaide

Adelaide is an ungrouped type 3 carbonaceous chondrite with the affinities to the CM and CO groups. However, it appears to have escaped thermal metamorphism and alteration (Fitzgerald and Jones, 1977; Davy et al., 1978; Kallemeyn and Wasson, 1982; Hutcheon and Steele, 1982; Kerridge, 1985; Huss and Hutcheon, 1992; Krot et al., 2001d; Huss et al., 2003).

AOAs comprise ~30% of all refractory inclusions identified in Adelaide (Krot et al., 2004a). They consist of forsterite ($Fa_{<2}$; Fig. 1l), weathered Fe, Ni-metal nodules, and CAIs composed of anorthite, Al-diopside, and spinel; no melilite was found (Fig. 24). There are significant variations in modal mineralogy of CAIs and forsterite/CAI ratios in AOAs. Spinel grains appear to be corroded to varying degrees by anorthite (Fig. 24). About 10% of AOAs contain low-Ca pyroxene that replaces forsterite along grains boundaries and around opaque nodules or form thick shells with abundant Fe, Ni-metal nodules around AOAs (Krot et al., 2004e; Fig. 25). No other secondary phases were found.

2.9. Overall mineral compositions of AOAs

Olivines in AOAs from primitive carbonaceous chondrites (CR, CH, CB, CM, Acfer 094, Adelaide, CO3.0) are nearly pure forsterite ($Fa_{<2}$); more fayalitic olivines occur in AOAs from meteorites which experienced alteration and metamorphism, such as CV_{oxA}, CV_{red}, and CO chondrites of petrologic types 3.1–3.9 (Fig. 1). Primary olivines in AOAs in the CV_{oxB} chondrites are compositionally similar to those in primitive carbonaceous chondrites, whereas secondary olivines approach to nearly pure fayalite. Olivine in AOAs from primitive carbonaceous chondrites has large ranges in MnO (up to 1.6 wt%) and Cr_2O_3 (up to 0.6 wt%) (Fig. 26). Some

Fig. 18. Combined X-ray elemental maps (a) in Mg (red), Ca (green), and Al *Kα* (blue), and (b) in Mg (red), Ca (green), and Si *Kα* (blue), and BSE images (c–f) of AOAs with low-Ca pyroxene in the CR chondrites PCA91082 (a–c), GRA95229 (d), and NWA 1180 (e,f). (a–c) AOA ♯24 contains ~50 vol% of CAIs surrounded by forsterite (fo); both components contain rounded inclusions of Fe, Ni-metal (mt). The CAIs largely consist of Al-diopside (di) and spinel (sp); anorthite (an) and melilite (mel) are minor. Low-Ca pyroxene (px; outlined in (c), (d), and (f)) replaces forsterite along grain boundaries and forms rims around Fe, Ni-metal nodules; it also occurs as subhedral grains intergrown with Fe, Ni-metal. Region outlined in (a) are shown in detail in (c). (d) AOA ♯17 is highly porous and contains low-Ca pyroxene associated with Fe, Ni-metal. (E) AOA ♯10 is a porous aggregate of forsterite, numerous, irregularly shaped CAIs composed of anorthite and minor Al-diopside, and Fe, Ni-metal grains. Low-Ca pyroxene replaces forsterite along grain boundaries and around Fe, Ni-metal nodules in the peripheral portion of the AOA. (F) AOA ♯5 is composed of forsterite, Fe, Ni-metal, Al-diopside and anorthite, and has a compact texture. Al-diopside occurs as subhedral and euhedral grains in anorthite, indicating crystallization from melt. Low-Ca pyroxene (outlined) occurs as a discontinuous layer in the outermost portion of the AOA.

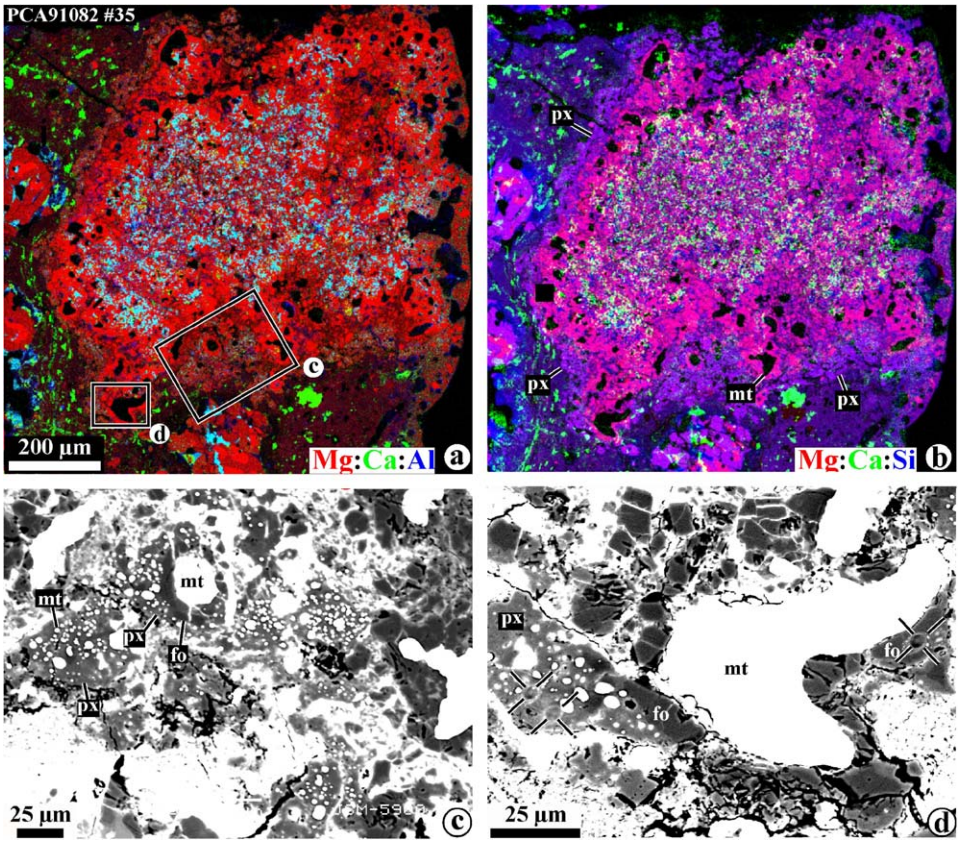


Fig. 19. Combined X-ray elemental maps (a) in Mg (red), Ca (green), and Al *Kα* (blue), and (b) in Mg (red), Ca (green), and Si *Kα* (blue), and BSE images (c,d) with low-Ca pyroxene in the CR chondrite PCA91082. The AOA consists of forsterite (fo), Fe, Ni-metal (mt), and CAIs (bluish in (a)) composed of anorthite, Al-diopside and minor spinel. AOA is mineralogically zoned: its core is enriched in Al-diopside and anorthite and depleted in Fe, Ni-metal relative to the forsterite-rich mantle; the mantle is surrounded by a continuous layer of low-Ca pyroxene (px) with abundant, tiny inclusions of Fe, Ni-metal. The pyroxene replaces olivine. Regions outlined in (a) are shown in detail in (c) and (d). Arrows in (d) indicate ion probe spots.

AOAs show zoned distribution in MnO and Cr_2O_3: olivines in the outer portions of AOAs are generally enriched in these elements compared to those in AOA cores (an. 3–5, Table 1). Compared to AOAs, olivines in Al-rich chondrules (ARCs) are slightly, but systematically enriched in Cr_2O_3, CaO and fayalite contents (Fig. 26). Olivines in AOA/ARC-like objects are enriched in CaO relative to those in AOAs (Fig. 26).

Plagioclase in AOAs is nearly pure anorthite (Table 2), whereas plagioclase grains in AOA/ARC-like objects and ARCs always have detectable Na_2O (Krot and Keil,

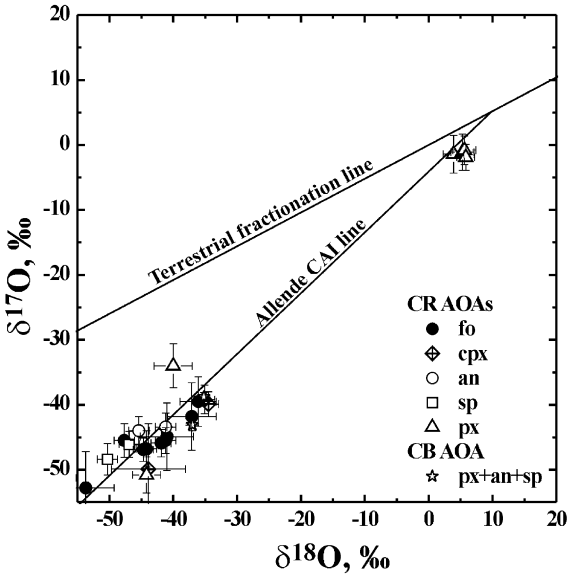


Fig. 20. Oxygen isotopic compositions (errors are 2σ) of individual minerals in AOAs from the CB and CR chondrites (data Aléon et al., 2002; Krot et al., 2004d). Forsterite (fo), anorthite (an), diopside (di), and spinel (sp) in the CR and CB AOAs are ^{16}O-rich; both ^{16}O-rich and ^{16}O-poor low-Ca pyroxenes (px) were found in CR AOAs.

2002; Krot et al., 2002c, 2004a, e). Melilite in AOAs is åkermanite-poor ($Åk_{<15–20}$) (Table 2). Spinel in AOAs from primitive chondrites is nearly pure $MgAl_2O_4$; spinel in AOAs from altered and metamorphosed chondrites is enriched in FeO (Table 3). Spinel in ARCs is systematically enriched in Cr_2O_3 compared to those in AOAs (Krot and Keil, 2002; Krot et al., 2002c).

High-Ca pyroxenes in AOAs have large ranges in Al_2O_3 (2–20 wt%) and TiO_2 (up to 13 wt%); MnO and Cr_2O_3 contents are generally below detection limits of electron microprobe analysis (Table 4; Fig. 27). High-Ca pyroxenes in ARCs have lower Al_2O_3, higher TiO_2, and significantly higher MnO and Cr_2O_3 contents than those in AOAs (Fig. 27). Low-Ca pyroxenes in AOAs have low Al_2O_3 (<2 wt%) and TiO_2 (<0.6 wt%), but detectable contents of MnO (0.7–0.6 wt%) and Cr_2O_3 (0.04–1.2 wt%) (Table 4; Fig. 27). Low-Ca pyroxenes in AOAs and AOA/ARC-like objects are compositionally similar to those in ARCs (Fig. 27).

Fe, Ni-metal grains were analyzed only in the CR and CH AOAs. Their compositions, together with those in cores and rims of the CR chondrules, are shown in Fig. 28. Most metal grains in the CR and CH AOAs have 5–7 wt% Ni and a solar Co/Ni ratio. In contrast to metal grains in chondrules, those in AOAs show no significant compositional variations within an individual AOA. A very Fe, Ni-metal-rich AOA shown in Fig. 17e and f is the only exception; its metal contains 7–12 wt% Ni.

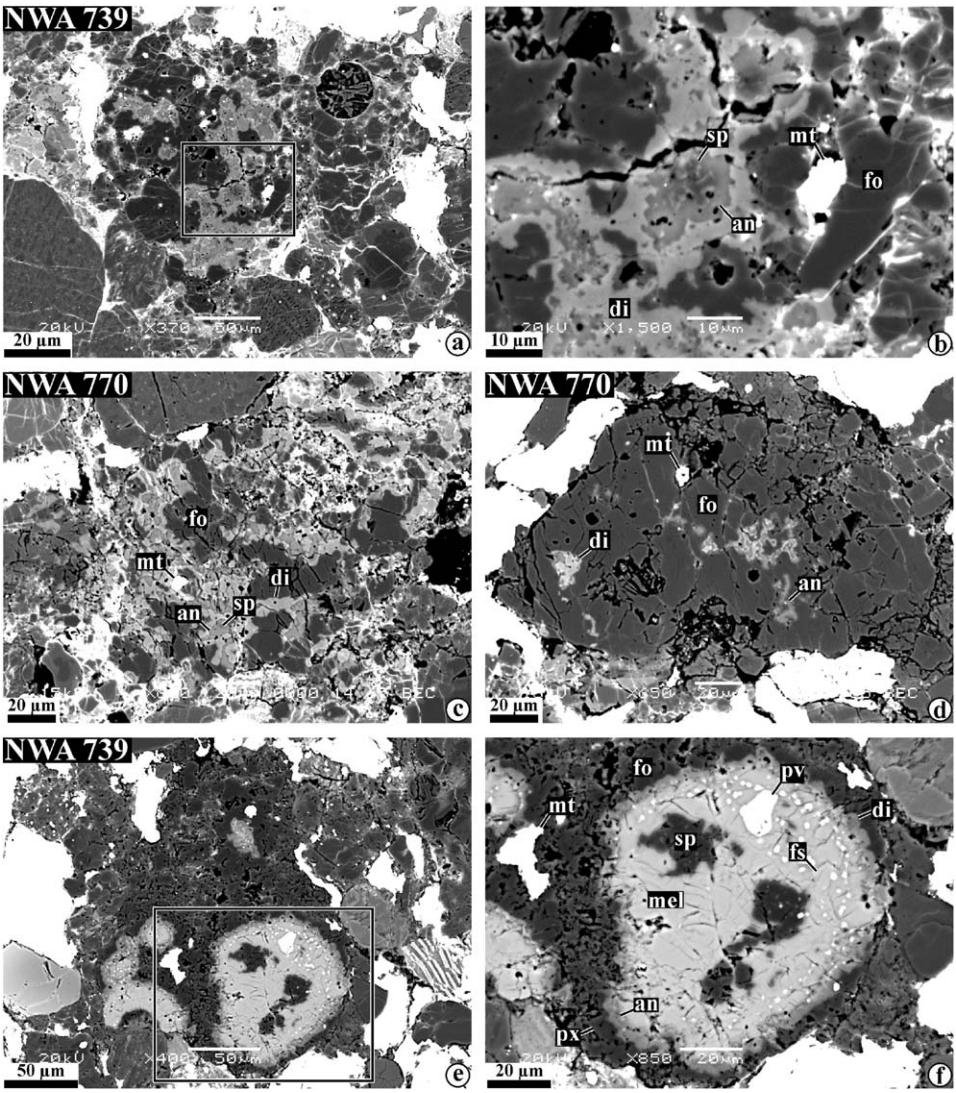


Fig. 21. BSE images of AOAs, in CH chondrites NWA 739 and NWA 770. (a–d) The AOAs consist of forsterite (fo), Fe, Ni-metall (mt), Al-diopside (di), anorthite (an), and minor spinel (sp), which corroded by anorthite. (e,f) AOA containing several compact, melilite-rich CAIs composed of melilite (mel), spinel, perovskite (pv), and fassaite (fs); melilite is slightly corroded by anorthite. The CAIs are surrounded by Al-diopside rims. Micron-size layers of low-Ca pyroxene (px) replace forsterite along grain boundaries.

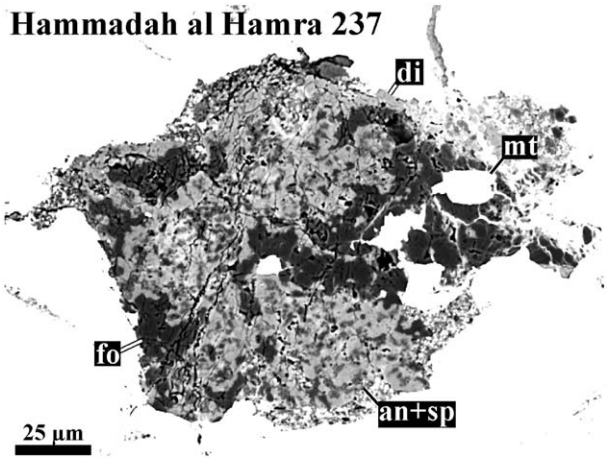


Fig. 22. BSE image of AOA in the CB_b chondrite Hammadah al Harma 237. It consists of forsterite (fo), Fe, Ni-metal (mt), and a refractory component composed of Al-diopside (di) and fine-grained intergrowths of anorthite (an) and spinel (sp).

3. Discussion

3.1. Summary of mineralogical and petrographic observations

AOAs in primitive chondrites consist of three major components: forsterite, Fe, Ni-metal, and CAIs composed of Al-diopside, anorthite, spinel, and very rare melilite independent from the chondrite group. There are significant variations in modal abundances of these components, as well as modal mineralogy and textures of the CAIs. Most AOAs are irregularly shaped, fine-grained and porous objects, which appear to have escaped extensive melting. Some AOAs are rounded, coarse-grained and compact, suggesting that they probably experienced thermal processing such as annealing and recrystallization or even melting. Although AOAs show no textural evidence for being completely melted, some CAIs in AOAs are rounded, compact objects, which probably crystallized from melts. These observations suggest that AOAs are aggregates of forsterite, Fe, Ni-metal and both igneous or non-igneous CAIs. Forsterite-rich accretionary rims around igneous and non-igneous CAIs in CR and CV chondrites have similar textures and mineralogy to AOAs and can be considered as AOAs with a dominant CAI component.

CAIs in AOAs are typically mineralogically zoned: their central zone consists of melilite $\pm$ spinel $\pm$ perovskite or spinel $\pm$ perovskite. Melilite, if present, is generally extensively replaced by a fine-grained, symplectitic intergrowth of spinel, Al-diopside, and, sometimes, anorthite (e.g., Figs. 6d and 17d). In the melilite-free CAIs, spinel is surrounded by a fine-grained, symplectitic intergrowth of spinel and Al-diopside (e.g., Fig. 10c) or by anorthite, encased in a monomineralic layer of

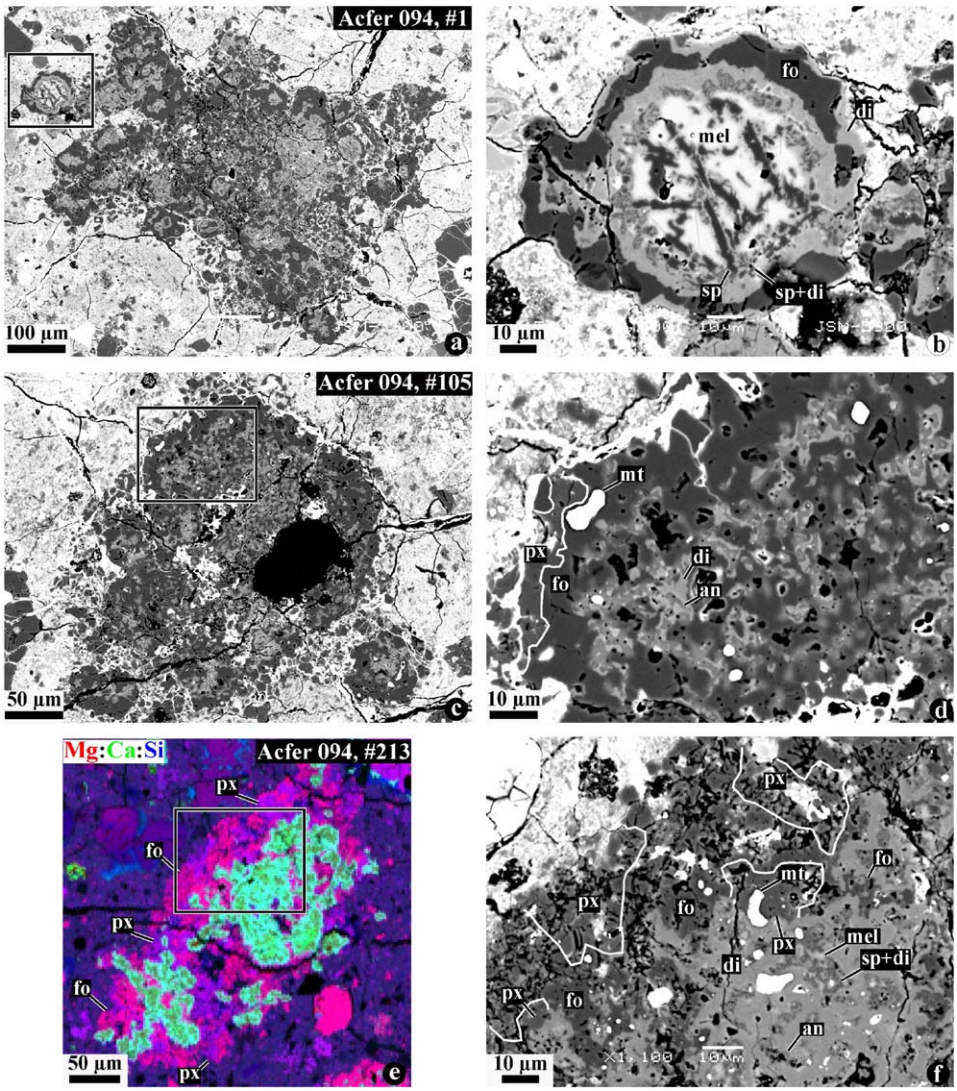


Fig. 23. BSE images (a–d, f) and combined X-ray elemental maps (e) in Mg (red), Si (green), and Al $K\alpha$ (blue) of AOAs in the ungrouped carbonaceous chondrite Acfer 094. The AOAs consist of forsteritic olivine (fo), Fe, Ni-metal (mt), ±low-Ca pyroxene (px) and CAIs composed of anorthite (an), Al-diopside (di), ±melilite (mel), ±spinel (sp). Melilite is typically replaced by symplectitic intergrowths of spinel and Al-diopside. Low-Ca pyroxene (bluish in (e); outlined in (d) and (f)) replaces forsterite in outer portions of the AOAs. Regions outlined in (a), (c), and (e) are shown in detail in (b), (d), and (f), respectively.

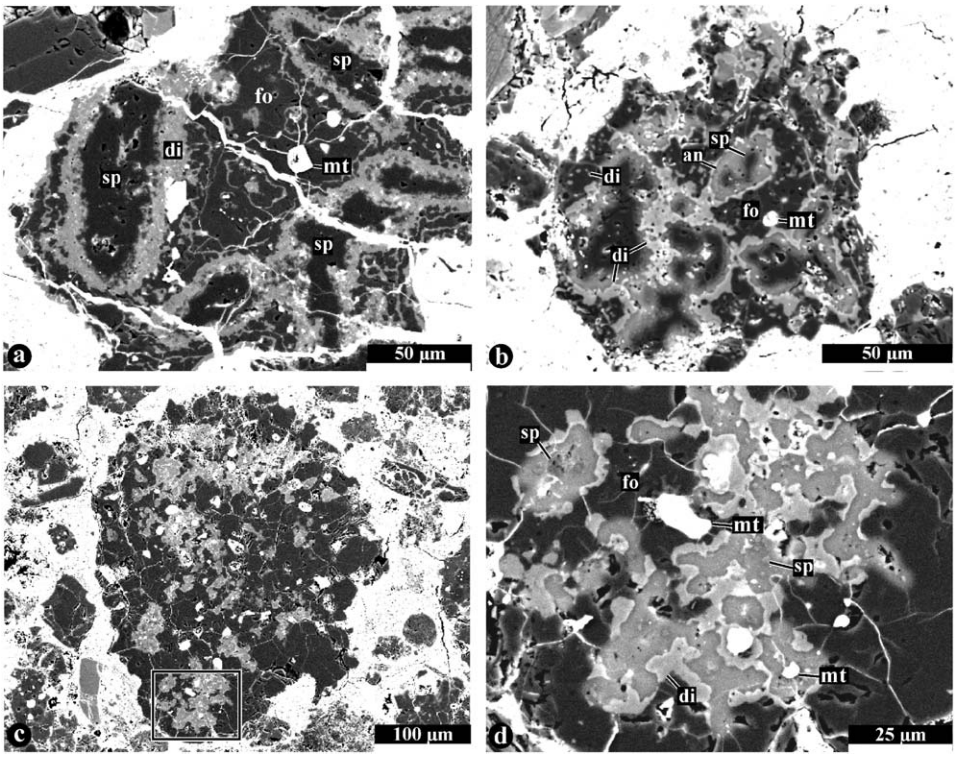


Fig. 24. (a–d) BSE images of AOAs in the ungrouped carbonaceous chondrite Adelaide. AOAs consist of forsterite (fo), Fe, Ni-metal (mt), and CAIs composed of Al-diopside (di), anorthite (an), and spinel (sp). The CAI/forsterite ratios and the modal mineralogy of CAIs vary in a broad range. Spinel is replaced by anorthite to a various degree. Region outlined in (c) is shown in detail in (d).

Al-diopside (e.g., Fig. 21b). There are corrosional relationships between spinel and the surrounding anorthite. The layer of Al-diopside often shows enrichment in Al towards the CAI cores (e.g., Fig. 17c); occasionally, it is overgrown by a compact forsterite layer (e.g., Fig. 5c). About 10% of AOAs contain small (<1–2 vol%) amounts of low-Ca pyroxene replacing forsterite. There are three major textural occurrences of low-Ca pyroxene in AOAs: (i) thin ($<10\,\mu m$) discontinuous layers along forsterite grain boundaries in AOA peripheries; (ii) haloes and subhedral grains around Fe, Ni-metal grains, which are largely concentrated in AOA peripheries, and (iii) thick (up to $70\,\mu m$) continuous layers, often with abundant tiny inclusions of Fe, Ni-metal grains, around AOAs.

The petrographic observations suggest the following formation sequence of minerals in AOAs: spinel $\rightarrow$ melilite $\rightarrow$ Al-diopside $\pm$ spinel $\pm$ anorthite $\rightarrow$ forsterite + Fe, Ni-metal $\rightarrow$ low-Ca pyroxene. Although mineralogical observations clearly show that the fine-grained, sympletictic intergrowths of Al-diopside, spinel, and

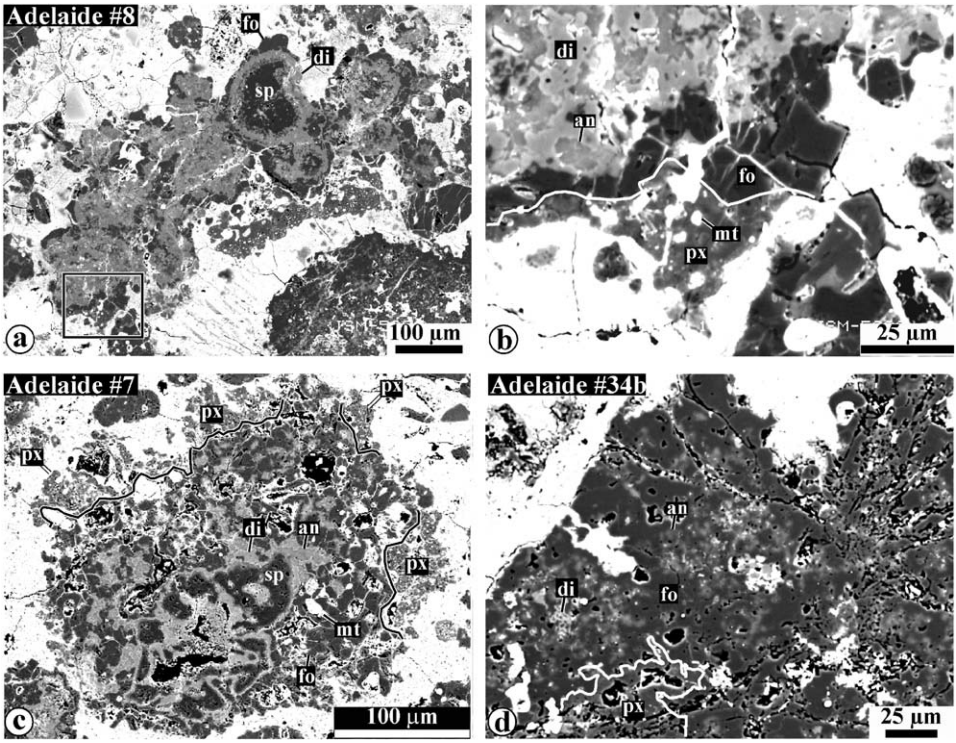


Fig. 25. BSE images of AOAs with low-Ca pyroxene in Adelaide. (a,b) AOA #8 is dominated by CAIs composed of Al-diopside (di), spinel (sp), and minor anorthite (an). Coarse spinel grains are corroded by Al-diopside and anorthite. CAIs are surrounded by the discontinuous layers of forsterite (fo) and low-Ca pyroxene (px). The low-Ca pyroxene layer is in corrosion relationship with the forsterite layer and contains abundant opaque inclusions (weathered Fe, Ni-metal) and rare, relict forsterite grains. Region outlined in (a) is shown in detail in (b). (c) AOA #7 consists of forsterite, spinel, anorthite, Al-diopside, and Fe, Ni-metal (mt). The spinel grains are anhedral and are corroded by anorthite that is separated from forsterite by a layer of Al-diopside. AOA is surrounded by a continuous layer, up to 50 μm in thickness, of low-Ca pyroxene (outlined) that corrodes forsterite and contains abundant, tiny inclusions of Fe, Ni-metal. (d) AOA #34b consists of porous forsterite-rich regions containing abundant very fine-grained anorthite and Al-diopside and surrounded by compact forsterite rims. Both occurrences of forsterite are replaced by low-Ca pyroxene (outlined).

anorthite occur as alteration products of melilite, this mineral assemblage is in general agreement with the thermodynamically predicted condensation sequence from a gas of solar composition at $P_{tot} = 10^{-5}$ bar[1] (Petaev and Wood, 1998a):

[1] At a total pressure of 10^{-3} bar, the condensation sequence is the same, except for the fact that Fe, Ni-metal condenses before forsterite, at 1462 and 1444 K, respectively (Yoneda and Grossman, 1995; Ebel and Grossman, 2000; Petaev et al., 2003; Krot et al., 2004e).

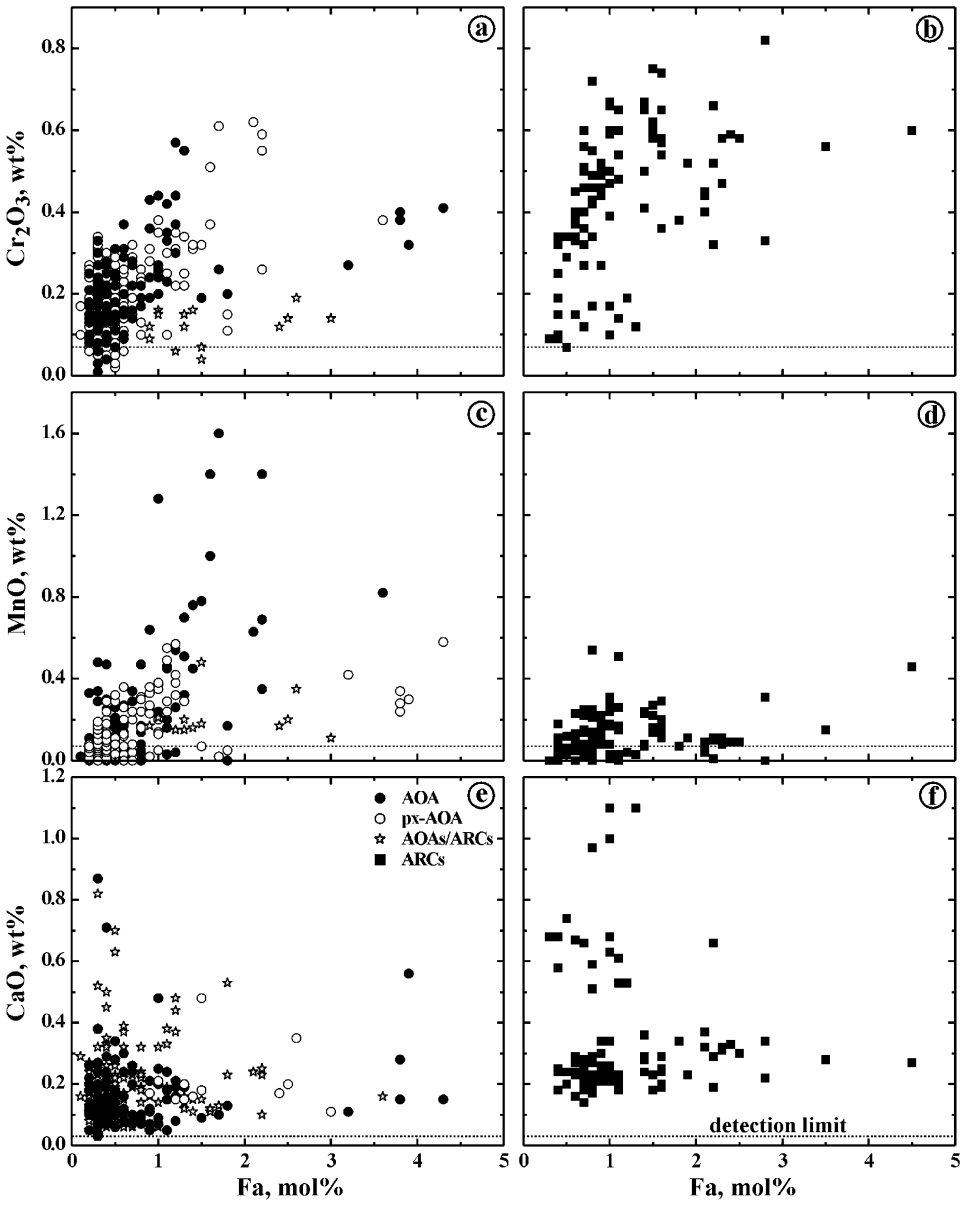


Fig. 26. Fayalite vs. Cr_2O_3 (a,b), MnO (c,d) and CaO (e,f) in olivines in AOAs with (px-AOA) and without (AOA) low-Ca pyroxene, objects intermediate between AOAs and Al-rich chondrules (ARCs), and ARCs in primitive carbonaceous chondrites. Dashed lines indicate detection limits of electron microprobe analyses.

Table 1. Representative electron microprobe analyses of olivine in AOAs

An. #	1	2	3	4	5	6	7	8	9	10
AOA #	213[a]	311[a]	209	209	209	8[a]	46[a]	35[a]	24[a]	20[a]
SiO_2	42.2	43.8	42.7	43.0	42.8	42.4	41.7	42.5	42.3	42.7
TiO_2	<0.09	<0.09	0.13	0.12	0.08	<0.09	<0.09	<0.09	0.12	<0.09
Al_2O_3	0.07	0.03	0.04	<0.03	<0.03	<0.03	<0.03	0.05	0.16	0.07
Cr_2O_3	0.14	0.31	0.31	0.28	0.38	0.22	0.51	0.52	0.17	<0.07
FeO	0.30	0.48	1.2	0.95	1.0	1.4	3.5	1.2	0.35	0.85
MnO	<0.07	0.29	0.54	0.64	1.3	0.18	0.29	0.32	<0.07	<0.07
MgO	57.0	56.5	55.5	56.4	55.4	55.1	53.4	56.2	56.5	56.5
CaO	0.18	0.06	0.44	0.16	0.14	0.32	0.18	0.22	0.19	0.10
Na_2O	<0.06	<0.06	<0.06	<0.06	<0.06	<0.06	<0.06	<0.06	<0.06	<0.06
K_2O	<0.04	<0.04	<0.04	<0.04	<0.04	<0.04	<0.04	<0.04	<0.04	<0.04
Total	99.9	101.5	100.9	101.6	101.1	99.6	99.6	101.0	99.8	100.2
Fa	0.3	0.5	1.2	0.9	1.0	1.4	3.5	1.1	0.4	0.8

An. #—analysis number; 1–5—Acfer 094 (ungrouped); 6, 7—Adelaide (ungrouped); 8, 9—PCA91082 (CR); 10—Efremovka (CV).

[a]AOAs with low-Ca pyroxene.

Table 2. Representative electron microprobe analyses of plagioclase and melilite in AOAs

An. #	1[a]	2[a]	3[a]	4	5	6	7	8	9
Min	pl	pl	pl	pl	pl	pl	pl	Mel	Mel
SiO_2	43.1	40.8	40.1	42.8	40.1	42.1	41.1	24.1	25.0
TiO_2	<0.09	<0.09	<0.09	0.25	<0.09	0.20	<0.09	<0.09	<0.09
Al_2O_3	37.2	36.6	39.0	34.6	39.0	36.4	38.0	32.8	32.7
Cr_2O_3	<0.07	<0.07	<0.07	<0.07	<0.07	<0.07	<0.07	<0.07	<0.07
FeO	0.27	0.71	0.11	0.28	0.11	0.30	0.46	0.34	0.25
MnO	<0.07	<0.07	<0.07	<0.07	<0.07	<0.07	<0.07	<0.07	<0.07
MgO	0.09	0.42	1.6	1.5	1.6	0.86	0.86	1.8	1.9
CaO	20.1	19.5	18.6	19.7	18.6	20.0	19.5	40.3	40.4
Na_2O	<0.06	<0.06	<0.06	<0.06	<0.06	0.07	0.07	<0.06	<0.06
K_2O	<0.04	<0.04	<0.04	<0.04	<0.04	<0.04	<0.04	0.05	<0.04
Total	100.8	98.1	99.3	99.1	99.3	99.9	99.9	99.4	100.3

An. #—analysis number; 1—Adelaide (ungrouped); 2, 8, 9—Acfer 094 (ungrouped); CRs: 2—EET87770; 4—MAC87320; 5—EET87770; 6, 7—GRA95229; min—mineral; pl—plagioclase; mel—melilite.

[a]AOAs with low-Ca pyroxene.

melilite (1503 K), spinel (1371 K), diopside (1323 K), forsterite (1318 K), anorthite (1293 K), FeNi-metal (1290 K), and orthopyroxene (1263 K),[2] implying that alteration of melilite took place at high temperatures in the nebula. In order to

[2]The appearance of melilite prior to spinel in the condensation sequence, contrary to petrographic observations, is a well-known problem that has not been solved yet (Yoneda and Grossman, 1995; Petaev and Wood, 1998a, b; Ebel and Grossman, 2000; Petaev et al., 2003).

Table 3. Representative electron microprobe analyses of spinel in AOAs

An. #	1	2	3	4[a]	5	6	7	8
SiO_2	0.08	0.08	0.14	0.08	0.17	<0.04	0.08	0.09
TiO_2	0.24	0.10	0.19	0.24	0.19	0.37	0.74	0.33
Al_2O_3	72.1	72.0	70.8	72.1	71.0	71.1	70.4	72.5
Cr_2O_3	0.16	0.15	0.54	0.16	0.41	0.18	0.55	0.46
FeO	0.16	0.45	0.14	0.16	0.21	0.13	0.26	0.13
MnO	<0.07	0.09	<0.07	<0.07	<0.07	<0.07	<0.07	<0.07
MgO	27.8	27.8	27.8	27.8	28.2	27.4	27.3	27.4
CaO	0.06	0.11	0.15	0.06	0.15	0.04	0.06	0.08
Na_2O	<0.06	<0.06	<0.06	<0.06	<0.06	<0.06	<0.06	<0.06
K_2O	<0.04	<0.04	<0.04	<0.04	<0.04	<0.04	<0.04	<0.04
Total	100.6	100.8	99.8	100.6	100.3	99.2	99.4	101.0

An. #—analysis number; 1—Adelaide (ungrouped); CRs: 2–4—PCA91082; 5—El Djouf 001; 6—EET87770; 7—GRA95229; 8—Gao-Guenie (b).

[a]AOA with low-Ca pyroxene.

Table 4. Representative electron microprobe analyses of low-Ca and high-Ca pyroxenes in AOAs

An. #	1	2	3	4	5	6	7	8	9	10	11	12	13	14
AOA #	7	213	46	35	24	7	7	213	8	8	46	24	24	24
min	px	px	px	px	px	cpx	cpx	cpx	cpx	cpx	cpx	cpx	cpx	cpx
SiO_2	58.5	57.9	57.5	57.5	59.4	52.2	49.5	53.4	52.4	42.3	52.8	32.2	49.5	54.5
TiO_2	0.30	<0.09	0.39	0.17	<0.09	1.5	2.4	<0.09	0.26	2.3	0.87	6.7	0.31	<0.09
Al_2O_3	0.85	0.21	1.1	2.0	0.58	2.8	7.5	3.4	2.8	15.7	4.8	27.8	9.3	1.3
Cr_2O_3	0.75	0.33	1.0	0.84	0.27	0.13	<0.07	0.11	<0.07	0.23	0.53	<0.07	0.09	<0.07
FeO	1.5	0.74	3.0	1.8	0.81	0.93	0.27	0.27	0.50	1.2	0.90	0.15	0.09	0.07
MnO	0.32	0.12	0.48	0.37	0.09	<0.07	<0.07	<0.07	<0.07	<0.07	0.11	<0.07	<0.07	<0.07
MgO	36.2	39.8	34.8	35.6	39.6	18.8	15.9	18.3	18.0	13.0	18.4	9.4	16.7	19.5
CaO	1.9	0.26	2.9	2.6	0.60	22.9	24.5	24.7	24.0	23.4	22.1	23.6	24.1	23.9
Na_2O	<0.06	<0.06	<0.06	<0.06	<0.06	<0.06	<0.06	<0.06	<0.06	<0.06	<0.06	<0.06	<0.06	<0.06
K_2O	<0.04	<0.04	<0.04	<0.04	<0.04	<0.04	<0.04	<0.04	<0.04	<0.04	<0.04	<0.04	<0.04	<0.04
Total	100.3	99.4	101.2	100.9	101.4	99.3	100.1	100.2	98.0	98.1	100.5	99.9	100.1	99.3
Fs	2.1	1.0	4.4	2.7	1.1	1.5	0.5	0.4	0.8	2.1	1.4	0.3	0.1	0.1
Wo	3.6	0.5	5.4	4.9	1.1	45.9	52.4	49.1	48.6	55.3	45.7	64.2	50.9	46.7

An. #—analysis number; 1, 2, 8–10—Acfer 094 (ungrouped); 3, 9–11—Adelaide (ungrouped); 4, 5, 12–14—PCA91082 (CR); min—mineral; px—low-Ca pyroxene; cpx—Al-diopside.

distinguish these high-temperature minerals from other secondary, apparently low-temperature, phases such as ferrous olivine, salite-hedenbergite pyroxenes, andradite, nepheline, sodalite, phyllosilicates, magnetite, carbonates and Fe, Ni-sulfides, observed only in AOAs from altered and metamorphosed chondrites, we call them "primary" and "secondary", respectively. The origins of primary and secondary mineralizations in AOAs are discussed in separate sections below.

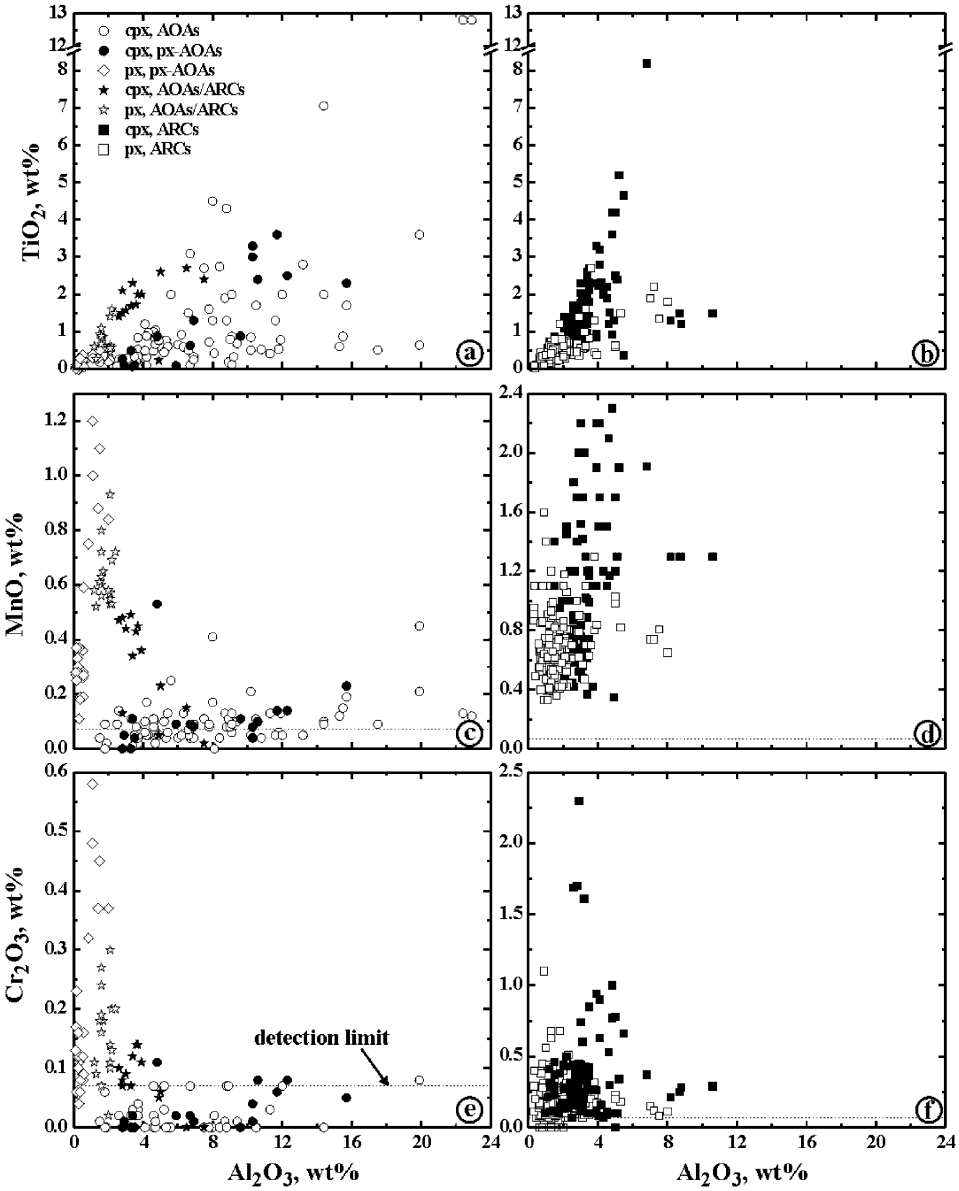


Fig. 27. Al_2O_3 vs. TiO_2 (a,b), MnO (c,d) and Cr_2O_3 (e,f) in low-Ca pyroxenes (px) and high-Ca pyroxenes (cpx) in AOAs, AOAs with low-Ca pyroxene (px-AOAs) and AOA/ARC-like objects (a, c, e) and Al-rich chondrules (b,d,f) in carbonaceous chondrites. Dashed lines indicate detection limits of electron microprobe analyses.

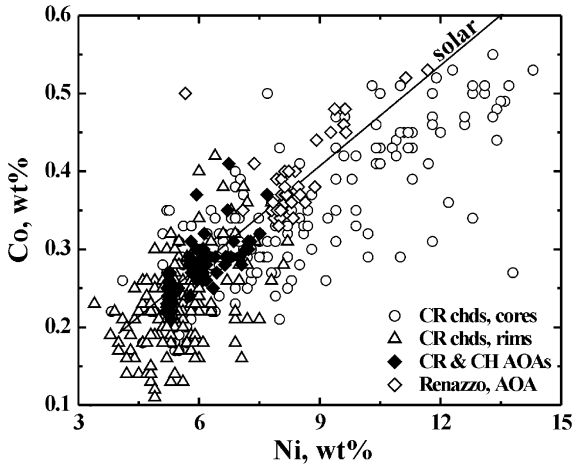


Fig. 28. Compositions of Fe, Ni-metal in the CR and CH AOAs and in cores and rims of the CR chondrules. Solar Co/Ni ratio is shown for reference. Metal grains in AOAs have approximately solar Co/Ni ratio. Most metal grains in AOAs have 5–7 wt% Ni; metal grains in the Renazzo AOA shown in Fig. 17(e and f) are enriched in Ni (7–12 wt%). Metal grains in chondrule cores are enriched in Ni relative to those in chondrule rims, suggesting evaporation and recondensation of Fe (Humayun et al., 2002).

3.2. High-temperature condensation reactions recorded by AOAs

The general similarity between the petrographic crystallization sequence of AOAs and the equilibrium condensation sequence of the gas of solar composition clearly points to the condensation origin of AOAs. However, there are some differences between the mineralogies of AOAs and the predicted equilibrium condensates that allow us to estimate modes of condensation in the nebular source region of AOAs. The most important difference is the presence of melilite, spinel, Al-diopside, anothite, forsterite, and $\pm$low-Ca pyroxene altogether in AOAs. Such a mineral assemblage is inconsistent with the equilibrium condensation model which predicts disappearance of melilite before condensation of forsterite begins. Obviously, retention of melilite in AOAs points to some degree of melilite isolation as predicted by the CWPI-type condensation (Petaev and Wood, 1998a). The intimate intergrowths of melilite and its alteration products, spinel, A-diopside, and anorthite, suggest that melilite was not physically isolated from the ambient nebular gas. It appears that it is the relatively fast cooling of the AOA's nebular source region that was responsible for cessation of melilite alteration. The reactions describing replacement of melilite by Al-diopside, spinel, and anorthite are discussed below, whereas the results of thermodynamic modeling of physicochemical conditions of melilite alteration are described in the section "*Thermodynamic analysis of condensation reactions recorded by AOAs*". Additional evidence in favor of condensate isolation during condensation of AOAs is listed below in the discussion of reactions responsible for mineralogy of AOAs.

Replacement of melilite by a fine-grained mixture of spinel, Al-diopside and ±anorthite observed in AOAs can be explained by reactions of melilite (gehlenite-åkermanite solid solution) with gaseous Mg and SiO:

$$Ca_2Al_2SiO_{7(s)} + 3SiO_{(g)} + 3Mg_{(g)} + 6H_2O_{(g)} \rightarrow 2CaMgSi_2O_{6(s)} + MgAl_2O_{4(s)} + 6H_{2(g)}, \quad (1)$$

$$Ca_2Al_2SiO_{7(s)} + 3SiO_{(g)} + Mg_{(g)} + 4H_2O_{(g)} \rightarrow CaAl_2Si_2O_{8(s)} + CaMgSi_2O_{6(s)} + 4H_{2(g)}. \quad (2)$$

Corrosion of spinel by anorthite and enrichment of diopside in Al towards anorthite could be explained by the following reaction:

$$MgAl_2O_{4(s)} + CaMgSi_2O_{6(s)} + 0.5SiO_{(g)} + 0.5H_2O_{(g)} \rightarrow 0.5CaAl_2Si_2O_{8(s)} + Mg_2SiO_{4(s)} + 0.5CaAl_2SiO_{6(s)} + 0.5H_{2(g)}. \quad (3)$$

In some cases, the corrosional appearance of spinel and enrichment of diopside in Al towards spinel are observed in nearly complete lack of anorthite (Fig. 5d in Komatsu et al., 2000). These observations can be explained by the reaction involving spinel and melilite:

$$3Ca_2Al_2SiO_{7(s)} + MgAl_2O_{4(s)} + 5SiO_{(g)} + Mg_{(g)} + 6H_2O_{(g)} \rightarrow [4CaAl_2SiO_6 + 2CaMgSi_2O_6]_{(px\ ss)} + 6H_{2(g)}. \quad (4)$$

Forsterite and Fe, Ni-metal must have formed by direct condensation from nebular gas according to the reactions:

$$2Mg_{(g)} + SiO_{(g)} + 3H_2O_{(g)} \rightarrow Mg_2SiO_{4(s)} + H_{2(g)}, \quad (5)$$

$$Fe_{(g)} + Ni_{(g)} \rightarrow Fe,\ Ni_{(ss)}. \quad (6)$$

The presence of low-Ca pyroxene replacing forsterite in the outer portions of AOAs is consistent with a condensation origin of low-Ca pyroxene from a cooling nebular gas:

$$Mg_2SiO_{4(s)} + SiO_{(g)} + H_2O_{(g)} \rightarrow Mg_2Si_2O_{6(s)} + H_{2(g)}. \quad (7)$$

The common occurrences of low-Ca pyroxene rims around Fe, Ni-metal nodules might indicate that Si dissolved in the metal was also involved in the reaction:

$$Mg_2SiO_{4(s)} + Si_{(in\ FeNi)} + 2H_2O_{(g)} \rightarrow Mg_2Si_2O_{6(s)} + 2H_{2(g)}. \quad (8)$$

The release of Si from Fe, Ni-metal to form low-Ca pyroxene according to reaction (8) is consistent with the predictions of the equilibrium condensation model. However, the high abundance of low-Ca pyroxene around Fe, Ni-metal along with the generally low Si contents in Fe, Ni-metal condensates (e.g., Petaev et al., 2003) suggest that this reaction is of minor importance in the formation of low-Ca pyroxene in AOAs.

The presence of thick low-Ca pyroxene shells with abundant FeNi-metal nodules around several AOAs may suggest (i) direct condensation of low-Ca pyroxene and

Fe, Ni-metal from nebular gas:

$$2Mg_{(g)} + 2SiO_{(g)} + 4H_2O_{(g)} \rightarrow Mg_2Si_2O_{6(s)} + 4H_{2(g)}, \quad (9)$$

(ii) reduction of ferrous silicates:

$$2(FeMg)SiO_{4(s)} + 2H_2O_{(g)} \rightarrow Mg_2Si_2O_{6(s)} + 2Fe_{(s)} + 2H_{2(g)}, \quad (10)$$

or (iii) accretion of pyroxene-normative material around AOAs, followed by melting. Direct condensation of low-Ca pyroxene (reaction (9)) is not predicted from a gas of solar composition (e.g., Yoneda and Grossman, 1995; Petaev and Wood, 1998a; Ebel and Grossman, 2000; Petaev et al., 2003) and would require existence of fractionated (Mg/Si < solar) gas. Such gas could have formed after isolation of forsterite either by its physical removal from the condensation region or by coarsening of forsterite condensates (Petaev and Wood, 1998a; Krot et al., 2002f). Our modeling of disequilibrium condensation (CWPI-type) in the nebula of solar composition at the isolation degree of 10 rel%/K shows that such a rapid and effective isolation of forsterite (e.g., in AOAs) will result in a large decrease of the Mg/Si ratio in the residual gas, leading to formation of small amounts of low-Ca pyroxene by reaction (7), followed by the direct condensation of low-Ca pyroxene (reaction (9)). Reduction of ferrous silicates (reaction (10)) is inconsistent with the petrographic observations, including the absence of ferrous silicates associated with CAIs or AOAs in primitive carbonaceous chondrites, the presence of Ni in metal in low-Ca pyroxene rims, and the lack of dusty relict grains in these rims.

Oxygen isotopic compositions of AOAs with different textural occurrences of low-Ca pyroxene provide additional constraints on the formation mechanisms of low-Ca pyroxene in AOAs. Low-Ca pyroxene replacing forsterite along grain boundaries and around Fe, Ni-metal nodules is ^{16}O-enriched to a level observed in forsterite of the host AOAs ($\Delta^{17}O < -20‰$), suggesting formation from the same gaseous reservoir. In contrast, thick low-Ca pyroxene ± Fe, Ni-metal shells are ^{16}O-depleted to a level commonly observed in carbonaceous chondrite chondrules ($\Delta^{17}O \sim 0‰$), suggesting formation in a different gaseous reservoir. The significance of oxygen isotopic compositions of AOAs for understanding oxygen isotopic compositions of the nebular gas is discussed below.

The relatively rare occurrences of low-Ca pyroxene in AOAs are apparently indicative either of the removal of AOAs from the hot nebular gas prior to condensation of low-Ca pyroxene, e.g., by a magneto-centrifugally driven stellar wind (Shu et al., 2001) or by a turbulent diffusion (Cuzzi et al., 2003), or of the kinetic inhibition of reaction (8) (Imae et al., 1993; Komatsu et al., 2000). From one hand, the lack of low-Ca pyroxene in many AOAs containing forsterite with significant MnO contents (Fig. 26; Weisberg et al., 2003) is apparently due to the sluggish kinetics of reaction (8), because Mn is predicted to condense after condensation of enstatite (e.g., Yoneda and Grossman, 1995; Ebel and Grossman, 2000; Petaev et al., 2003). From the other, the very presence of ^{16}O-rich low-Ca pyroxene in some MnO-poor AOAs (Fig. 26) clearly shows that reaction (8) did occur in the nebular reservoir enriched in ^{16}O. It appears that both the removal of

AOAs from their nebular source regions and the sluggish kinetics of reaction (8) were responsible for the lack of low-Ca pyroxene in most AOAs.

3.3. Thermodynamic analysis of condensation reactions recorded by AOAs

We can explore physicochemical conditions of the mineral reactions observed in the AOAs by modeling metasomatic interaction of solid inclusions injected into a system with solar bulk composition. The residual gaseous phase of such a system is assumed to be in equilibrium with the solid phases condensed out of the system. We further assume an open-system type of interaction between the AOAs and the surrounding gaseous phase, i. e., the amounts Si, Mg, Ca, H, and O added to or subtracted from the AOAs by reactions (1)–(4) do not change the partial pressures of Ca, Mg, SiO, H_2O, and H_2 in the gaseous system due to very low mass ratio of AOAs to the gaseous phase. The chemical compositions of the residual gaseous phase are calculated using CWPI code (Petaev and Wood, 2000; Petaev et al., 2003).

Out of the nine important mineral reactions written above, reactions (5)–(8) describe direct condensation of forsterite, metal, low-Ca pyroxene from the nebular gas; the $P-T$ conditions of these reactions were modeled directly by the CWPI code. Reaction (9) can take place only in a system with highly fractionated Mg and Si; such conditions have already been discussed above. Therefore, only reactions (1)–(4) are included in the thermodynamic analysis. The equations linking the equilibrium constants of these reactions ($\lg K_i$) with the partial pressures of gaseous species (lg[Mg], lg[SiO], lg[H_2O/H_2], and lg[Ca]) and activities of end-members of clinopyroxene (lg[Di], lg[CATS]) and melilite (lg[Gel], lg[Åk]) mineral solid solutions are as follows:

$$\lg K_1 = 2\lg[\mathrm{Di}] - \lg[\mathrm{Gel}] - 3\lg[\mathrm{Mg}] - 3\lg[\mathrm{SiO}] - 6\lg[\mathrm{H_2O/H_2}], \quad (11)$$

$$\lg K_2 = \lg[\mathrm{Di}] - \lg[\mathrm{Gel}] - \lg[\mathrm{Mg}] - 3\lg[\mathrm{SiO}] - 4\lg[\mathrm{H_2O/H_2}], \quad (12)$$

$$\lg K_3 = 0.5\lg[\mathrm{CATS}] - \lg[\mathrm{Di}] - 0.5\lg[\mathrm{SiO}] - 0.5\lg[\mathrm{H_2O/H_2}], \quad (13)$$

$$\lg K_4 = 2\lg[\mathrm{Di}] + 4\lg[\mathrm{CATS}] - 3\lg[\mathrm{Gel}] - 5\lg[\mathrm{SiO}] - \lg[\mathrm{Mg}] - 6\lg[\mathrm{H_2O/H_2}]. \quad (14)$$

Numerical values of equilibrium constants of reactions (1)–(4) were calculated using the thermodynamic database of the CWPI code. The values of standard thermodynamic properties of minerals and gaseous species involved in the reactions are from Chase (1998), Berman (1988), Sack and Ghiorso (1994), and Robie and Hemingway (1995). The melilite solid solution was treated as non-ideal (Charlu et al., 1981). Ignoring small amounts of $MgAl_2SiO_6$, $CaTi^{4+}Al_2O_6$, and $CaTi^{3+}AlSiO_6$, clinopyroxene was treated as an ideal solution of Ca-Tschermakite (CATS), $CaAl_2SiO_6$, and diopside, $CaMgSi_2O_6$ (Sack and Ghiorso, 1994). Calculations were done in the temperature range of 1000–1600 K and the pressure range of 10^{-3}–10^{-8} bar.

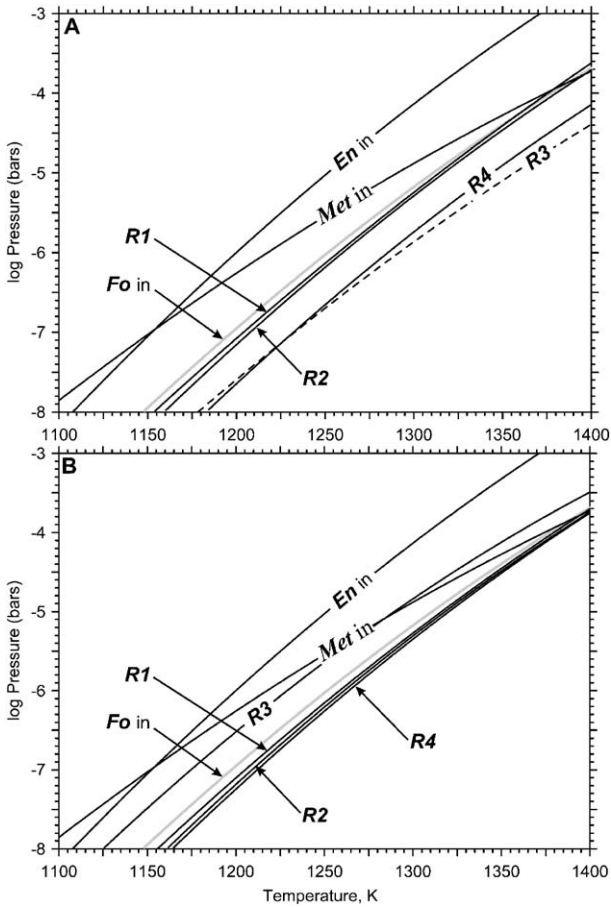


Fig. 29. Equilibrium condensation curves of some minerals and phase boundaries of reactions (1)–(4) (labeled as R1–R4) equilibrated with the residual nebular gas in a system of solar composition. Labels on the curves correspond either to the appearance of forsterite (*Fo* in), enstatite (*En* in), and FeNi-metal (*Met* in) or to reaction numbers. The stability fields of melilite are on the right-hand sides of the numbered curves. (A) Compositions of coexisting melilite and clinopyroxene are (Ge_{95}Åk$_5$) and ($Di_{95}CATS_5$), respectively. Dashed line shows the boundary of metastable reaction (3). (B) Compositions of coexisting melilite and clinopyroxene are (Ge_{95}Åk$_5$) and ($Di_{80}CATS_{20}$), respectively (from Krot et al., 2004e).

The results of thermodynamic analysis are shown in Fig. 29 as the log P vs. T plot. In calculating the positions of phase boundaries on these plots, all parameters of Eqs. (10)–(13) were replaced with numerical values either calculated using the CWPI code (partial pressures of gaseous species) or measured in the fine-grained inclusions studied. The compositions of mineral solid solutions used in the analysis are Al-rich

melilite ($Ge_{95}Åk_5$), Al-poor diopside ($Di_{95}CATS_5$), and Al-enriched diopside ($Di_{80}CATS_{20}$).

Phase boundaries of the alteration reactions (1)–(4) are shown at two different compositions of diopside—Al-poor (Fig. 29A) and Al-enriched (Fig. 29B). The major difference between the two diagrams is the positions of phase boundaries of reactions (3) and (4) that are highly dependent upon the Al content in diopside. The melilite stability fields are on the right hand side of all phase boundaries. Also plotted are the condensation curves of forsterite (reaction (5)), enstatite (reaction (7)) and Fe, Ni-metal (reaction (6)) that show that the alteration of melilite should occur before the condensation of Fe, Ni-metal and low-Ca pyroxene. This is consistent with the general lack of both minerals in the refractory component of AOAs. Because all phase boundaries are essentially parallel to each other, the alteration sequence is fairly independent of nebular pressure, although the absolute temperatures of the reactions are.

At the earliest stages of melilite alteration, probably even before the aggregation of CAIs and forsterite into AOAs, the assemblage of melilite and spinel will be replaced by the Al-poor diopside (reaction (4) in Fig. 29A). Because reaction (4) produces twice as much Ca-Tcshermakite as diopside, the concentration of the former will gradually increase as reaction (4) proceeds. Given enough time, reaction (4) would be the only alteration reaction until the concentration of CATS in clinopyroxene increases to >20 mole %, when formation of anorthite by reaction (2) becomes possible. Soon after, a direct replacement of melilite by a mixture of diopside and spinel (reaction (1)) may occur. At the conditions above, reaction (3) is metastable until the appearance of forsterite. However, a wide range of Al_2O_3 concentrations in Al-diopside (Table 4) suggests that neither reaction has reached an equilibrium state.

If the alteration process has started after the aggregation of the refractory component and forsterite into AOAs, all these reactions could have proceeded simultaneously until the complete disappearance of melilite. After that, only reaction (3) will take place resulting in a gradual disappearance of spinel, an increase in anorthite abundance, and an enrichment of diopside in Al. If reaction (3) is completed, the final equilibrium mineral assemblage of AOAs—forsterite, Al-diopside, and anorthite—would be quite similar (except for SiO_2 and small amounts of alkalies) to that of Type I chondrules. Fig. 29 clearly shows that the low-Ca pyroxene found in some AOAs formed much later, when the alteration of the refractory component of AOAs has completed. AOAs with low-Ca pyroxene always contain Fe, Ni-metal associated with forsterite. In the system of solar composition, the forsterite-metal and enstatite-metal reversals occur at nebular pressures of $\sim 7 \times 10^{-5}$ and $\sim 1 \times 10^{-7}$ bar (Fig. 29), which define the pressure range of metal-bearing AOAs with low-Ca pyroxene.

3.4. Low-temperature alteration of AOAs

Petrographic observations indicate that ferrous olivine, Ca, Fe-rich pyroxenes, andradite, nepheline, sodalite, phyllosilicates, magnetite, carbonates and Fe,

Ni-sulfides in AOAs are the late-stage, secondary minerals postdating crystallization of high-temperature, primary minerals described in Sections "*High-temperature condensation reactions recorded by AOAs*" and "*Thermodynamic analysis of condensation reactions recorded by AOAs*". They occur in AOAs from altered or metamorphosed chondrites, such as CVs, CRs, CMs, and CO chondrites of petrologic types 3.1–3.9, and are similar to secondary minerals reported in other chondritic components of their host meteorites (Brearley, 2004 and references therein). For example, AOAs, CAIs, chondrules and matrices in CR and CM chondrites contain phyllosilicates and $\pm$carbonates. All chondritic components in the CV_{oxB} chondrites contain ferrous olivine ($Fa_{>90}$) and phyllosilicates, whereas those in the CV_{oxA} chondrites contain less ferrous olivine ($Fa_{\sim 40–60}$), nepheline, and sodalite; Ca, Fe-rich pyroxenes, andradite, magnetite, and Fe, Ni-sulfides occur in both subgroups. These observations suggest that (i) secondary minerals in AOAs are products of alteration that affected all chondritic components of their host meteorites, favoring, but not proving, an asteroid setting of alteration. (ii) Secondary minerals in any chondritic component can be used to constrain conditions and environments of alteration; e.g., the presence of fayalite veins crosscutting fine-grained rims around chondrules in CV_{oxB} chondrites provides strong evidence for an asteroid origin of fayalite in their chondrules, CAIs, AOAs and matrices (Krot et al., 2004b).

There is a general agreement that aqueous alteration responsible for the formation of phyllosilicates, carbonates, magnetite, and Fe, Ni-sulfides in CM, CR, and CV_{oxB} chondrites occurred on their parent asteroids or on planetesimals of earlier generations (e.g., Brearley, 2004 and references therein). In contrast, the origin of anhydrous secondary minerals, e.g., ferrous olivine, nepheline, sodalite, Ca, Fe-rich pyroxenes, and andradite, in CO and CV chondrites remains controversial; both nebular and asteroid models have been proposed.

According to the nebular models (Palme and Wark, 1988; Kimura and Ikeda, 1995, 1998; Weisberg and Prinz, 1998; Dohmen et al., 1998), chondritic components in the oxidized CV and metamorphosed CO chondrites were exposed to a highly oxidized, high-temperature, nebular gas and altered by this gas. The anhydrous secondary minerals, such as nepheline, sodalite, and magnetite, formed by replacement of primary minerals, such as anorthite, glassy mesostasis, melilite, and Fe, Ni-metal; ferrous olivine, Ca, Fe-rich pyroxenes and andradite condensed directly from this gas. The nebular models are, however, inconsistent with (i) the petrographic evidence for asteroid alteration experienced by the CV chondrites and their dark inclusions, including veins and chondrule pseudomorphs composed of ferrous olivine, nepheline, Fe, Ni-sulfides, and Ca, Fe-rich silicates, Ca, Fe-rich rims around dark inclusions, talc and amphibole in Allende chondrules (e.g., Fruland et al., 1978; Kojima and Tomeoka, 1996; Buchanan et al., 1997; Krot et al., 1997, 1998a, b, 2000, 2001e, 2004b; Brearley, 1997), (ii) the presence of poorly graphitized carbon and pentlandite inclusions in matrix olivine, which are unstable at high temperatures (Brearley, 1999), (iii) the lack of volatility-controlled REE patterns in Ca, Fe-pyroxenes and andradite in the Allende matrix (Brearley and Shearer, 2000), (iv) the large ($\delta^{18}O \sim 20‰$) mass-dependent fractionation of oxygen isotopes in

secondary fayalite, magnetite, Ca, Fe-rich pyroxenes, and andradite, all having similar values of $\Delta^{17}O$ ($\sim 0‰$ to $-2‰$), suggesting that alteration occurred at low temperatures in a similar O-isotopic reservoir (Krot et al., 2000; Choi et al., 2000; Cosarinsky et al., 2003), (v) the prolonged duration (~ 14 Ma) of alteration of CV chondrites (Pravdivtseva and Hohenberg, 2001; Pravdivtseva et al., 2001, 2003a, b; Krot et al., 2003c), which is inconsistent with the inferred shorter (5–10 Ma) life-time of the solar nebula (Podosek and Cassen, 1994) and (vi) the thermodynamic analysis of condensation of ferrous olivine from the high-temperature nebular gas (Grossman and Fedkin, 2003).

According to the asteroid models (Kojima and Tomeoka, 1996; Rubin, 1998; Krot et al., 1995, 1998a, 2004b; Chizmadia et al., 2002; Itoh and Tomeoka, 2003a, b), CV and CO chondrites experienced a fluid-assisted thermal metamorphism to varying degrees that resulted in mobilization of Ca, Si, Fe, Mg, Mn, Na, and S via an aqueous solution. Nepheline, sodalite, and magnetite formed by replacement of primary phases, such as anorthite, melilite, and Fe, Ni-metal. Ferrous olivine and Ca, Fe-rich silicates formed by several mechanisms, including replacement of magnetite, replacement of magnesian olivine and pyroxene, and direct precipitation from an aqueous solution.

The abundance of secondary nepheline and ferrous olivine ($Fa_{>50}$) in CAIs, chondrules, and AOAs in CO chondrites is correlated with the degree of thermal metamorphism experienced by their host meteorites, favoring an asteroid setting of alteration (e.g., Russell et al., 1998; Rubin, 1998; Chizmadia et al., 2002; Itoh and Tomeoka, 2003b). Although the exact mechanism of nepheline formation remains unclear (e.g., Itoh and Tomeoka, 2003b), the apparent loss of refractory lithophile elements, such as Ca, from primary minerals in chondrules, CAIs, and AOAs replaced by nepheline, must require the presence of an aqueous solution, e.g.:

$$2Na^{+}_{(aq)} + CaAl_2Si_2O_{8(s)} \rightarrow 2NaAlSiO_{4(s)} + Ca^{2+}_{(aq)}. \quad (15)$$

Calcium released during this reaction could have been used to form secondary Ca, Fe-rich silicates, commonly observed in CV chondrites (e.g., Fig. 4), possibly by the following reactions:

$$Ca^{2+}_{(aq)} + Fe^{2+}_{(aq)} + 2SiO_{2(aq)} + 2H_2O_{(l,g)} \rightarrow CaFeSi_2O_{6(s)} + 2H_{2(g)}, \quad (16)$$

$$3Ca^{2+}_{(aq)} + Fe_3O_{4(s)} + 6SiO_{2(aq)} + 2H_2O_{(l,g)} \rightarrow 3CaFeSi_2O_{6(s)} + 2H_{2(g)}, \quad (17)$$

$$Ca^{2+}_{(aq)} + SiO_{2(aq)} + H_2O_{(l,g)} \rightarrow CaSiO_{3(s)} + H_{2(g)}. \quad (18)$$

An asteroid origin of Ca, Fe-rich silicates during a fluid-assisted thermal metamorphism on the CV asteroid was originally proposed by Krot et al. (1998b) and was later supported by textural observations (MacPherson and Krot, 2002), trace element (Brearley and Shearer, 2000) and oxygen isotopic studies (Krot et al., 2000; Cosarinsky et al., 2003) of Ca, Fe-rich silicates in chondrules, CAIs, and matrices of the oxidized CV chondrites.

The presence of subhedral and euhedral ferrous olivine grains coexisting with Fe, Ni-sulfides and phyllosilicates and overgrowing forsterite without significant Fe–Mg interdiffusion in AOAs in the CV_{oxB} chondrites (Fig. 4; Krot et al., 2004b) suggests a low-temperature origin of ferrous olivine. Low-temperature formation of ferrous olivine is also supported by the presence of ferrous olivine veins and chondrule pseudomorphs in the CV and CO chondrites and their dark inclusions (e.g., Krot et al., 2001e; Ohnishi and Tomeoka, 2002; Itoh and Tomeoka, 2003a). Because growth of ferrous olivine in FeO-free AOAs requires transport of moderately volatile elements such Fe, Mg, Si, and Mn, at low temperatures it can be only achieved by an aqueous solution. Based on the petrographic observations, oxygen (Choi et al., 2000; Hua et al., 2003) and chromium (Hutcheon et al., 1998; Hua et al., 2002) isotopic studies, and a thermodynamic analysis, Krot et al. (2004b) concluded that secondary ferrous olivine in the oxidized CV chondrites formed by replacement of magnetite:

$$2Fe_3O_{4(s)} + 3SiO_{2(aq)} + 2H_{2(g)} \rightarrow 3Fe_2SiO_{4(s)} + 2H_2O_{(l,g)} \quad (19)$$

by replacement of magnesian olivine and pyroxene:

$$Fe^{2+}_{(aq)} + Mg_2SiO_{4(s)} + H_2O_{(l,g)} \rightarrow (Fe,Mg)_2SiO_{4(s)} + Mg^{2+}_{(aq)} + H_{2(g)}, \quad (20)$$

$$Fe^{2+}_{(aq)} + MgSiO_{3(s)} + H_2O_{(l,g)} \rightarrow (Fe,Mg)_2SiO_{4(s)} + H_{2(g)} \quad (21)$$

and by direct precipitation from an aqueous solution:

$$Fe^{2+}_{(aq)} + Mg^{2+}_{(aq)} + SiO_{2(aq)} \rightarrow (Fe,Mg)_2SiO_{4(s)}. \quad (22)$$

Precipitation of ferrous olivine from an aqueous solution followed by thermal metamorphism has been also invoked by Chizmadia et al. (2002) and Imai and Yurimoto (2003) to explain mineralogical and oxygen isotopic observations of AOAs in metamorphosed CO and CV_{oxA} chondrites.

3.5. Oxygen isotopic compositions of AOAs: implication for understanding oxygen isotopic reservoirs in the solar nebula and on asteroids

Primary minerals (forsterite, Al-diopside, spinel, anorthite) in AOAs from the CM, CR, CB, and CO3.0 chondrites are uniformly ^{16}O-enriched (Figs. 12, 16 and 20). Low-Ca pyroxenes replacing forsterite along grain boundaries and around Fe, Ni-metal are similarly ^{16}O-enriched, whereas those forming thick, compact shells around AOAs are ^{16}O-depleted. These observations and the inferred condensation origin of primary minerals in AOAs discussed above suggest that AOAs formed in an ^{16}O-rich ($\Delta^{17}O < -20‰$) gaseous reservoir (Krot et al., 2002b). Because non-igneous CAIs in these chondrite groups have similarly ^{16}O-rich isotopic compositions, but are more refractory than AOAs, we infer that the ^{16}O-rich gaseous reservoir was dominant throughout the entire temperature range of condensation of minerals in CAIs and AOAs (i.e., from corundum, $T_{cond} \sim 1700$ K at $P_{tot} = 10^{-5}$ bar to low-Ca pyroxene, $T_{cond} \sim 1300$ K at $P_{tot} = 10^{-5}$ bar). Short-lived isotope chronometry of AOAs can potentially resolve the spatial vs. temporal existence of

such reservoir in the solar nebula. Although limited studies of ^{26}Al–^{26}Mg systematics of AOAs (Imai and Yurimoto, 2003) appear to support the existence of such reservoir in the early solar nebula (Krot et al., 2002b), more work is needed to confirm this conclusion. The ^{16}O-poor low-Ca pyroxene shells around ^{16}O-rich CAIs must have resulted from melting of solids that accreted around AOAs reflecting subsequent thermal processing of AOAs in an ^{16}O-poor gaseous reservoir, probably during chondrule formation (Krot et al., 2004b, e).

Low-temperature secondary minerals (nepheline, sodalite, ferrous olivine, phyllosilicates) as well as primary anorthite and, occasionally, Al-diopside, in AOAs from CV chondrites show varying degrees of depletion in ^{16}O relative to forsterite and spinel, which are enriched in ^{16}O to the levels observed in AOAs from primitive carbonaceous chondrites (Fig. 3). Forsterite in the accretionary rims around CV CAIs is also ^{16}O-rich, whereas the host CAIs show oxygen isotopic heterogeneity, with melilite being ^{16}O-depleted relative to spinel, hibonite, and Al-diopside (Fig. 9). The ^{16}O-rich compositions of forsterite, spinel, and in most cases, Al-diopside, in CV AOAs further support our conclusion on the existence of a ^{16}O-rich gaseous reservoir in the solar nebula. The observed oxygen isotope heterogeneities in the CV AOAs probably reflect subsequent thermal processing either in the solar nebula or on the CV parent asteroid.

The ^{16}O-poor compositions of ferrous olivine in the CV AOAs (Fig. 3) that probably formed by fluid-rock interaction suggest the existence of a ^{16}O-poor reservoir on the CV parent asteroid. This conclusion is supported by the ^{16}O-poor compositions of (i) fayalite and magnetite in Type I chondrules and matrices of the CV_{oxB} chondrites (Choi et al., 2000; Hua et al., 2003), (ii) Ca, Fe-rich silicates precipitating in pore space of the forsterite-rich accretionary rims (Hiyagon, 1998; Cosarinsky et al., 2003) and in rims around Allende dark inclusions (Krot et al., 2000), and (iii) nepheline and phyllosilicates replacing primary minerals in the CV AOAs (Imai and Yurimoto, 2003). Anorthite in AOAs from the CV_{oxA} chondrites is ^{16}O-depleted relative to anorthite in AOAs from the reduced CVs, possibly indicating isotope exchange during alteration on the CV asteroid (Imai and Yurimoto, 2003; Fagan et al., 2004). This model can be potentially tested by studying anorthite in AOAs from CO chondrites of different petrologic subtypes. It has been previously shown that oxygen isotopic compositions of melilite in CAIs from CO chondrites are correlated with petrologic subtypes of their host meteorites, suggesting an asteroid setting of oxygen isotopic exchange (Wasson et al., 2001). No oxygen isotopic measurements of anorthite or melilite in AOAs from metamorphosed CO chondrites have yet been reported.

The observed variations in oxygen isotopic compositions of Al-diopside in some unaltered AOAs from the reduced CV chondrites could have resulted from transient heating events to temperatures of about 1100–1300°C in a nebular setting, possibly during chondrule formation (Fagan et al., 2004). Additional argument favoring oxygen isotope exchange in the solar nebula comes from the study of the extensively melted AOA from Efremovka that preserved ^{16}O-rich signature only in spinel; forsterite, high-Ca pyroxene and anorthite in this AOA are ^{16}O-poor (Krot et al., 2004d).

3.6. Relationship between CAIs, AOAs, aluminum-rich and ferromagnesian chondrules

Our petrographic observations indicate that AOAs are genetically related to spinel–pyroxene–anorthite CAIs, commonly associated with AOAs. The limited mineralogical variations of CAIs in AOAs (spinel, pyroxene, anorthite, and minor melilite) are probably due to their fine-grained nature favoring continuous reactions with the cooling nebular gas (largely SiO_2 and MgO), which resulted in replacement of higher-temperature condensates by the lower-temperature mineral assemblage (see Section "*High-temperature condensation reactions recorded by AOAs*"). Forsterite-rich, accretionary rims around CAIs are texturally, mineralogically and isotopically similar to AOAs, suggesting a similar nature. However, CAIs surrounded by these rims are larger, more compact and more refractory than those in AOAs and the rims themselves. This probably reflects the lower degrees of nebular reactions experienced by these CAIs.

In spite of the common presence of forsterite-rich, accretionary rims around igneous (Type B) CAIs, the forsterite-bearing Type B CAIs are exceptionally rare (e.g., MacPherson et al., 1988). These observations may indicate that either melting of CAIs occurred largely prior to condensation of forsterite (i.e., at higher ambient nebular temperatures) or that CAI melts experienced extensive volatilization of Mg and Si (e.g., Grossman et al., 2002).

CAIs in AOAs are mineralogically similar to fine-grained, spinel-rich CAIs ("fine-grained CAIs" hereafter); however, there are some differences between these objects as well. Fine-grained CAIs are aggregates of multiple concentrically zoned objects composed of spinel cores surrounded by melilite and/or anorthite, and Al-diopside layers; most of them have group II REE patterns. Although AOAs have also an aggregational nature, CAIs inside them show no evidence for being aggregates and typically have unfractionated REE patterns. Although these observations may suggest that fine-grained CAIs and AOAs formed in different nebular regions, the limited number of REE measurements of AOAs, makes this conclusion uncertain. For example, the presence of forsterite-rich, accretionary rims around some fine-grained CAIs in CV chondrites contradicts this scenario.

In order to explore a potential genetic relationship between spinel–pyroxene–anorthite CAIs, AOAs and chondrules, bulk compositions of spinel–pyroxene–anorthite CAIs and AOAs from CR, CH, Adelaide and Acfer 094, together with magnesian (Type I and Al-rich) chondrules from LL3.0 Semarkona (Jones and Scott, 1989), Acfer 094 (Krot et al., 2004a), Adelaide (Krot et al., unpubl.), CRs (Weber and Bischoff, 1997; Krot and Keil, 2002), CB_b (Krot et al., 2001c) and CVs (Sheng et al., 1991; Krot et al., 2002c), are plotted on a projection from spinel onto the plane Ca_2SiO_4–Mg_2SiO_4–Al_2O_3 of the CaO–MgO–Al_2O_3–SiO_2 system (Fig. 30; MacPherson and Huss, 2003). Bulk compositions of AOAs on this diagram occupy a region between anorthite, diopside, and forsterite, consistent with their mineralogy. Bulk compositions of Al-rich chondrules composed of Al-diopside ± spinel ± forsterite overlap with those of spinel–pyroxene–anorthite CAIs, suggesting that Al-diopside-rich, Al-rich chondrules could have been formed by melting of such CAIs. Bulk compositions of Al-rich chondrules composed of plagioclase, low-Ca and high-Ca

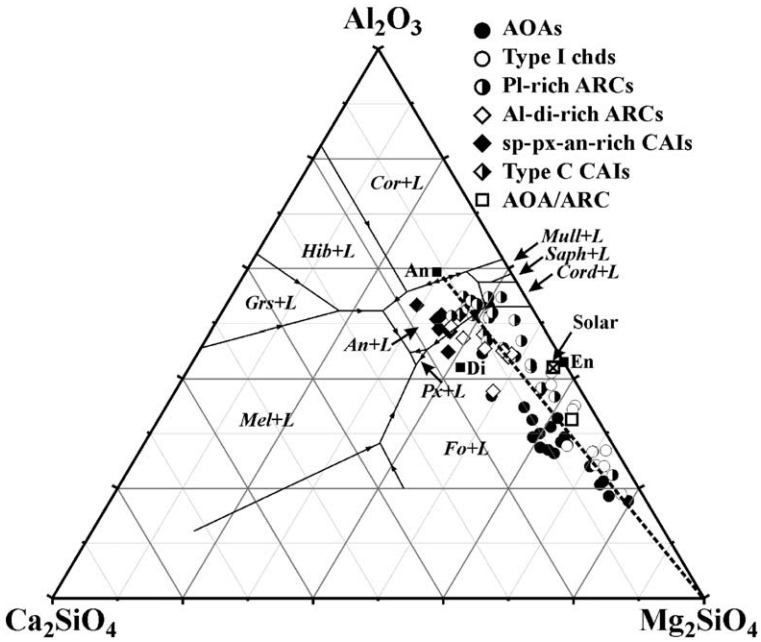


Fig. 30. Bulk compositions of AOAs, igneous (Type C) and non-igneous spinel–pyroxene–anorthite (sp–px–an-rich) CAIs, Type I ferromagnesian chondrules, Al-rich, plagioclase-rich (Pl-rich ARCs) chondrules, Al-rich, Al-diopside-rich (Al-di-rich ARCs) chondrules, and an object intermediate between AOA and Al-rich chondrule (AOA/ARC), projected from spinel onto the plane Ca_2SiO_4–Mg_2SiO_4–Al_2O_3 (MacPherson and Huss, 2003). Data from Jones and Scott (1989), Sheng et al. (1991), Komatsu et al. (2000), Krot and Keil (2002), and Krot et al. (2001b, 2002c, 2004e). An—anorthite, Cor—corundum, Cord—cordierite, En—enstatite, Fo—forsterite, Di—diopside, Grs—grossite, Hib—hibonite, L—liquid, Mel—melilite, Mull—mullite, Px—pyroxene, and Saph—saphirine.

pyroxenes, forsterite, and ±spinel and of Type I chondrules occupy a region to the right from the forsterite–anorthite thermal divide, whereas those of spinel–pyroxene–anorthite CAIs and AOAs plot to the left from it. This precludes formation of plagioclase-rich, Al-rich chondrules and Type I chondrules from AOAs or CAIs by an igneous fractionation. A similar conclusion was reached by Komatsu et al. (2000) based on the differences in mineral chemistry of AOAs and plagioclase-rich, Al-rich chondrules. Formation of low-Ca pyroxene by reaction of AOAs with gaseous SiO or melting of AOAs surrounded by a pyroxene-rich dust moves the bulk compositions of the AOAs across the thermal divide, providing a possible mechanism of transformation of refractory objects into chondrules. This mechanism is supported by the discovery of extensively melted AOAs with low-Ca pyroxene shells around them (Krot et al., 2004d, e). These objects have bulk compositions similar to chondrules, but preserved the original ^{16}O-rich signature in the unmelted spinel grains.

4. Future work

This review revealed some gaps in studies of AOAs, including limited data on bulk trace element abundances, nearly complete absence of ^{26}Al–^{26}Mg measurements, lack of oxygen isotopic data on AOAs in several primitive meteorites, including Acfer 094, Adelaide, and CH chondrites, and lack of microtextural studies. Trace element measurements can potentially provide important constraints on relationships between AOAs and chondrules. The ^{26}Al–^{26}Mg studies are important for the understanding of the ^{26}Al distribution in the early solar nebula, which is crucial for its chronological implication. For example, many hibonite-rich and grossite-rich CAIs lack $^{26}Mg^*$, which may reflect either their late-stage thermal processing or a heterogeneous distribution of ^{26}Al in the CH CAI-forming region (Weber et al., 1995). Since AOAs in CH chondrites appear to have escaped melting, their ^{26}Al–^{26}Mg studies can potentially provide an answer to this question. If it is found that AOAs in primitive chondrites have always a canonical $(^{26}Al/^{27}Al)_0$ ratio, studies of AOAs that experienced extensive melting (e.g., AOA/ARC objects) can answer the question on timing of this melting, which is possibly a chondrule-forming event. Transmission electron microscopy (TEM) studies of pristine AOAs can potentially provide crucial information on the degrees of melting experienced by AOAs and the mechanisms of growth of low-Ca pyroxene. TEM studies of AOAs from altered meteorites can help to distinguish between low-temperature and high-temperature formation of secondary minerals, such as fayalite, Ca, Fe-rich pyroxenes, nepheline, and sodalite.

5. Conclusions

1. Amoeboid olivine aggregates (AOAs) are the most common type of refractory inclusions in CM, CR, CH, CV, CO, and ungrouped carbonaceous chondrites Acfer 094 and Adelaide; only one AOA was found in the CB_b chondrite Hammadah al Hamra 237 and none were observed in the CB_a chondrites Bencubbin, Gujba, and Weatherford.
2. In primitive (unaltered and unmetamorphosed) carbonaceous chondrites, AOAs consist of forsterite ($Fa_{<2}$), Fe, Ni-metal, and Ca, Al-rich inclusions (CAIs) composed of Al-diopside, spinel, anorthite, and very rare melilite. Melilite is typically replaced by a fine-grained mixture of spinel, Al-diopside, and $\pm$anorthite; spinel is replaced by anorthite. About 10% of AOAs contain low-Ca pyroxene replacing forsterite. AOAs have similar textures and mineralogy to those of forsterite-rich accretionary rims surrounding different types of CAIs (compact and fluffy Type A, Type B, and fine-grained, spinel-rich) in CV and CR chondrites.
3. Forsterite and spinel in AOAs and forsterite-rich, accretionary rims are always ^{16}O-rich ($\delta^{17,18}O \sim -40‰$ to $-50‰$), whereas melilite, anorthite, and, occasionally, diopside could be either similarly ^{16}O-rich or ^{16}O-depleted to

varying degrees; the latter is relatively common in AOAs from altered and metamorphosed carbonaceous chondrites such as CV and CO3.1–3.9. Low-Ca pyroxene has either ^{16}O-rich ($\delta^{17,18}O \sim -40‰$) or ^{16}O-poor ($\delta^{17,18}O \sim 0‰$) isotopic compositions.

4. Most AOAs in CV chondrites have unfractionated ($\sim 2–10 \times$ CI) REE patterns. The initial $^{26}Al/^{27}Al$ ratios in AOAs in Y-81020 (CO3.0) are close to a canonical value of $4–5 \times 10^{-5}$.
5. AOAs in CH, CO3.0, Acfer 094 and Adelaide show no evidence for alteration. Secondary mineralizations in AOAs from CR, CM, and CO3.1–3.9, and CV chondrites are similar to those in other chondritic components of their host meteorites and include phyllosilicates, magnetite, carbonates, nepheline, sodalite, grossular, wollastonite, hedenbergite, andradite, and ferrous olivine.
6. We infer that AOAs and forsterite-rich, accretionary rims formed in ^{16}O-rich gaseous reservoir as aggregates of solar nebular condensates originally composed of forsterite, Fe, Ni-metal, and CAIs. Some of the CAIs were melted prior to aggregation and experienced formation of WLRs. Before and probably after the aggregation, melilite and spinel in CAIs reacted with SiO and Mg of the solar nebula gas enriched in ^{16}O to form Al-diopside and anorthite. Forsterite in some AOAs reacted with ^{16}O-enriched SiO gas to form low-Ca pyroxene. Some other AOAs were subsequently reheated and melted to varying degrees in an ^{16}O-poor gaseous reservoir, possibly during chondrule formation. The most extensively melted AOAs experienced oxygen isotope exchange with ^{16}O-poor nebular gas and may have been transformed into magnesian chondrules.
7. Secondary mineralizations and at least some of the oxygen isotope exchange in AOAs from altered and metamorphosed chondrites must have resulted from alteration in the presence of aqueous solutions after aggregation and lithification of the chondrite parent asteroids.

Acknowledgements

This work was supported by NASA grants NAGW5-10610 and NAG5-13131 (A.N. Krot, PI), NAG5-11591 (K. Keil, P.I.), NAG5-11546 (M.K. Weisberg, P.I.), RFBR 02-05-64859 and Program "Universities of Russia" A.A. Ulyanov, P.I.). We thank Dr. H. Connoly and Dr. A. Greshake for comprehensive reviews of the manuscript, comments and suggestions. This is Hawai'i Institute of Geophysics and Planetology publication No. 1340 and School of Ocean and Earth Science and Technology publication No. 642.

References

Aléon, J., Krot, A.N., McKeegan, K.D., 2002. Ca–Al-rich inclusions and amoeboid olivine aggregates from the CR carbonaceous chondrites. Meteorit. Planet. Sci. 37, 1729–1755.

Bar-Matthews, M., MacPherson, G.J., Grossman, L., 1979. An SEM-petrographic study of amoeboid olivine aggregates in Allende (abstract). Meteoritics 14, 342.

Berman, R.G., 1988. Internally consistent thermodynamic data for minerals in the system Na_2O–K_2O–CaO–MgO–FeO–Fe_2O_3–Al_2O_3–SiO_2–TiO_2–H_2O–CO_2. J. Petrol. 29, 445–522.
Brearley, A.J., 1997. Disordered biopyriboles, amphibole, and talc in the Allende meteorite: products of nebular or parent body aqueous alteration? Science 276, 1103–1105.
Brearley, A.J., 1999. Origin of graphitic carbon and pentlandite in matrix olivines in the Allende meteorite. Science 285, 1380–1382.
Brearley, A.J., 2004. Nebular versus parent body processing. In: Davis, A. (Ed.), Treatise on Geochemistry. Elsevier Press, Amsterdam, pp. 247–269.
Brearley, A.J., Shearer, C.K., 2000. Origin of calcium–iron-rich pyroxenes in Allende matrix: clues from rare-earth-element abundances (abstract). Meteorit. Planet. Sci. 35 (Suppl.), A33.
Buchanan, P.C., Zolensky, M.E., Reid, A.M., 1997. Petrology of Allende dark inclusions. Geochim. Cosmochim. Acta 61, 1733–1743.
Charlu, T.V., Newton, R.C., Kleppa, O.J., 1981. Thermochemistry of synthetic $Ca_2Al_2SiO_7$ (gehlenite)–$Ca_2MgSi_2O_7$ (åkermanite) melilites. Geochim. Cosmochim. Acta 45, 1609–1617.
Chase Jr., M.W., 1998. NIST-JANAF Thermodynamic Tables, 4th Edition. J. Phys. Chem. Ref. Data Monogr. No. 9, pp. 7951.
Chizmadia, L.J., Rubin, A.E., Wasson, J.T., 2002. Mineralogy and petrology of amoeboid olivine inclusions in CO3 chondrites: relationship to parent-body aqueous alteration. Meteorit. Planet. Sci. 37, 1781–1796.
Choi, B.-G., Krot, A.N., Wasson, J.T., 2000. Oxygen-isotopes in magnetite and fayalite in CV chondrites Kaba and Mokoia. Meteorit. Planet. Sci. 35, 1239–1249.
Clayton, R.N., Onuma, N., Grossman, L., Mayeda, T.K., 1977. Distribution of the pre-solar components in Allende and other carbonaceous chondrites. Earth Planet. Sci. Lett. 34, 209–224.
Cosarinsky, M., Leshin, L.A., MacPherson, G.J., Krot, A.N., Guan, Y., 2003. Oxygen isotope composition of Ca–Fe-rich silicates in and around al Allende Ca–Al-rich inclusion (abstract). Lunar Planet. Sci. XXXIV, Lunar Planet. Inst., CD-ROM #1043.
Cuzzi, J.N., Davis, S.S., Dobrovolskis, A.R., 2003. Formation and distribution of CAIs in the protoplanetary nebula (abstract). Lunar Planet. Sci. XXXIV, Lunar Planet. Inst., CD-ROM #1749.
Davy, R., Whitehead, S.G., Pitt, G., 1978. The Adelaide meteorite. Meteoritics 13, 121–139.
Dohmen, R., Chakraborty, S., Palme, H., Rammensee, W., 1998. Solid–solid reactions mediated by a gas phase: An experimental study of reaction progress and the role of surfaces in the system olivine + iron metal. Am. Miner. 83, 970–984.
Ebel, D.S., Grossman, L., 2000. Condensation in dust-enriched systems. Geochim. Cosmochim. Acta 64, 339–366.
Fagan, T.J., Krot, A.N., Keil, K., Yurimoto, H., 2004. Oxygen isotopic compositions of amoeboid olivine aggregates in the reduced CV3 chondrites Efremovka, Vigarano and Leoville. Geochim. Cosmochim. Acta 68, 2591–2611.
Fitzgerald, M.J., Jones, J.B., 1977. Adelaide and Bench Crater—members of a new subgroup of the carbonaceous chondrites. Meteoritics 12, 443–458.
Fruland, R.M., King, A.E., McKay, D.S., 1978. Allende dark inclusions. Proc. Lunar Sci. Conf. 9, 1305–1329.
Greshake, A., 1997. The primitive matrix components of the unique carbonaceous chondrite Acfer 094: a tem study. Geochim. Cosmochim. Acta 61, 437–452.
Grossman, L., Fedkin, A.V., 2003. Elemental abundance constraints on condensation of Allende matrix olivine (abstract). NIPR Symposium on Evolution of Solar System Materials: A New Perspective from Antarctic Meteorites, Tokyo, Japan, 31–32.
Grossman, L., Steele, I.M., 1976. Amoeboid olivine aggregates in the Allende meteorite. Geochim. Cosmochim. Acta 40, 149–155.
Grossman, L., Ganapathy, R., Methot, R.L., Davis, A.M., 1979. Trace elements in the Allende meteorite amoeboid olivine aggregates. Geochim. Cosmochim. Acta 43, 817–829.
Grossman, L., Ebel, D.S., Simon, S.B., 2002. Formation of refractory inclusions by evaporation of condensate precursors. Geochim. Cosmochim. Acta 66, 145–161.
Hashimoto, A., Grossman, L., 1987. Alteration of Al-rich inclusions inside amoeboid olivine aggregates in the Allende meteorite. Geochim. Cosmochim. Acta 51, 1685–1704.
Hiyagon, H., 1998. Distribution of oxygen isotopes in and around some refractory inclusions from Allende (abstract). Lunar Planet. Sci. XXIX, Lunar Planet. Inst., CD-ROM #1582.
Hiyagon, H., 2000. An ion microprobe study of oxygen isotopes in some inclusions in Kainsaz and Y-81020 CO3 chondrites (abstract). NIPR. Symp. Antarctic Meteorit. 25, 19–21.

Hiyagon, H., Hashimoto, A., 1999a. ^{16}O Excesses in olivine inclusions in Yamato-86009 and Murchison chondrites and their relation to CAIs. Science 283, 828–831.

Hiyagon, H., Hashimoto, A., 1999b. An ion microprobe study of oxygen isotopes in various types of inclusions in Y-82050 (CO3), ALHA77307 (CO3) and Y-86009 (CV3) chondrites (abstract). Lunar Planet. Sci. XXX, Lunar Planet. Inst., CD-ROM ♯1319.

Hiyagon, H., Hashimoto, A., 1999c. An ion microprobe study of oxygen isotopes in various types of inclusions in Yamato-791717 (CO3) chondrite: oxygen isotopes vs. fayalite content in olivine (abstract). NIPR. Symp. Antarctic Meteorit. 24, 37–39.

Hua, X., Buseck, P.R., 1995. Fayalite in the Kaba and Mokoia carbonaceous chondrites. Geochim. Cosmochim. Acta 59, 563–579.

Hua, X., Huss, G.R., Sharp, T.G., 2002. ^{53}Mn–^{53}Cr dating of fayalite formation in the Kaba CV3 carbonaceous chondrite (abstract). Lunar Planet. Sci. XXXIII, Lunar Planet. Inst., CD-ROM ♯1660.

Hua, X., Huss, G.R., Tachibana, S., Sharp, T.G., 2003. Oxygen isotopic compositions of fayalite in the Kaba CV3 carbonaceous chondrite (abstract). Lunar Planet. Sci. XXXIV, Lunar Planet. Inst., CD-ROM ♯1702.

Humayun, M., Campbell, A.J., Zanda, B., Bourot-Denise, M., 2002. Formation of Renazzo chondrule metal inferred from siferophile elements (abstract). Lunar Planet. Sci. XXXIII, Lunar Planet. Inst., CD-ROM ♯1965.

Huss, G.R., Hutcheon, I.D., 1992. Abundant $^{26}Mg^*$ in Adelaide refractory inclusions (abstract). Meteoritics 27, 236.

Huss, G.R., Hutcheon, I.D., Krot, A.N., Tachibana, S., 2003. Oxygen isotopes in refractory inclusions from the Adelaide carbonaceous chondrite (abstract). Lunar Planet. Sci. XXXIV, Lunar Planet. Inst., CD-ROM ♯1802.

Hutcheon, I.D., Steele, I.M., 1982. Refractory inclusions in the Adelaide carbonaceous chondrite (abstract). Lunar Planet. Sci. XXIII, Lunar Planet. Inst., 352–353.

Hutcheon, I.D., Krot, A.N., Keil, K., Phinney, D.L., Scott, E.R.D., 1998. ^{53}Mn–^{53}Cr dating of fayalite formation in the CV3 chondrite Mokoia: evidence for asteroidal alteration. Science 282, 1865–1867.

Imae, N., Tsuchiyama, A., Kitamura, M., 1993. An experimental study of enstatite formation reaction between forsterite and Si-rich gas. Earth Planet. Sci. Lett. 118, 21–30.

Imai, H., Yurimoto, H., 2003. Oxygen isotopic distribution in an amoeboid olivine aggregate from the Allende CV chondrite: primary and secondary processes. Geochim. Cosmochim. Acta 67, 765–772.

Itoh, D., Tomeoka, K., 2003a. Dark inclusions in CO3 chondrites: new indicators of parent-body processes. Geochim. Cosmochim. Acta 67, 153–169.

Itoh, D., Tomeoka, K., 2003b. Nepheline formation in chondrules in CO_3 chondrites: relationship to parent-body thermal metamorphism (abstract). NIPR Symposium on Evolution of Solar System Materials: A New Perspective from Antarctic Meteorites, Tokyo, Japan, 45–46.

Itoh, S., Rubin, A.E., Kojima, H., Wasson, J.T., Yurimoto, H., 2002. Amoeboid olivine aggregates and AOA-bearing chondrule from Y-81020 CO3.0 chondrite: distribution of oxygen and magnesium isotopes (abstract). Lunar Planet. Sci. XXXIII, Lunar Planet. Inst., CD-ROM ♯1490.

Jones, R.H., Scott, E.R.D., 1989. Petrology and thermal history of type IA chondrules in the Semarkona (LL3.0) chondrite. Proc. Lunar Planet. Sci. Conf. 19, 523–536.

Kallemeyn, G.W., Wasson, J.T., 1982. The compositional classification of chondrites: III. Ungrouped carbonaceous chondrites. Geochim. Cosmochim. Acta 46, 2217–2228.

Keller, L.P., Buseck, P.R., 1990. Aqueous alteration in the Kaba CV3 carbonaceous chondrite. Geochim. Cosmochim. Acta 54, 2113–2120.

Keller, L.P., Thomas, K.L., Clayton, R.N., Mayeda, T.K., DeHart, J.M., McKay, D.S., 1994. Aqueous alteration of the Bali CV3 chondrite: evidence from mineralogy, mineral chemistry, and oxygen isotopic compositions. Geochim. Cosmochim. Acta 58, 5589–5598.

Kerridge, J.F., 1985. Carbon, hydrogen and nitrogen in carbonaceous chondrites; abundances and isotopic compositions in bulk samples. Geochim. Cosmochim. Acta 49, 1707–1714.

Kimura, M., Ikeda, Y., 1995. Anhydrous alteration of Allende chondrules in the solar nebula: II, alkali-Ca exchange reactions and formation of nepheline, sodalite and Ca-rich phases in chondrules. Proc. NIPR Symp. Antarctic Meteorit. 8, 123–138.

Kimura, M., Ikeda, Y., 1998. Hydrous and anhydrous alterations of chondrules in Kaba and Mokoia CV chondrites. Meteorit. Planet. Sci. 33, 1139–1146.

Kojima, T., Tomeoka, K., 1996. Indicators of aqueous alteration and thermal metamorphism on the CV3 parent body: microtextures of a dark inclusion from allende. Geochim. Cosmochim. Acta 60, 2651–2666.

Komatsu, M., Krot, A.N., Petaev, M.I., Ulyanov, A.A., Keil, K., Miyamoto, M., 2000. Mineralogy and petrography of amoeboid olivine aggregates from the reduced CV3 chondrites Efremovka, Leoville and Vigarano: products of nebular condensation and accretion. Meteorit. Planet. Sci. 36, 629–643.

Kornacki, A.S., Wood, J.A., 1984a. Petrography and classification of Ca, Al-rich and olivine-rich inclusions in the Allende CV3 chondrite. J. Geophys. Res. 89, B573–B587.

Kornacki, A.S., Wood, J.A., 1984b. The mineral chemistry and origin of inclusion matrix and meteorite matrix in the Allende CV3 chondrite. Geochim. Cosmochim. Acta 48, 1663–1676.

Krot, A.N., Scott, E.R.D., Zolensky, M.E., 1995. Mineralogical and chemical modification of components in CV3 chondrites: nebular or asteroidal processing? Meteoritics 30, 748–775.

Krot, A.N., Scott, E.R.D., Zolensky, M.E., 1997. Origin of fayalitic olivine rims and plate-like matrix olivine in the CV3 chondrite Allende and its dark inclusions. Meteoritics 32, 31–49.

Krot, A.N., Petaev, M.I., Scott, E.R.D., Choi, B.-G., Zolensky, M.E., Keil, K., 1998a. Progressive alteration in CV3 chondrites: more evidence for asteroidal alteration. Meteorit. Planet. Sci. 33, 1065–1085.

Krot, A.N., Zolensky, M.E., Keil, K., Scott, E.R.D., Nakamura, K., 1998b. Secondary Ca–Fe-rich minerals in the Bali-like and Allende-like oxidized CV3 chondrites and Allende dark inclusions. Meteorit. Planet. Sci. 33, 623–645.

Krot, A.N., Hiyagon, H., Petaev, M.I., Meibom, A., 2000. Oxygen isotopic compositions of secondary Ca–Fe-rich silicates from the Allende dark inclusions: evidence against high-temperature formation (abstract). Lunar Planet. Sci. XXXI, Lunar Planet. Inst., CD ROM ♯1463.

Krot, A.N., Huss, G.R., Hutcheon, I.D., 2001a. Corundum-hibonite refractory inclusions from Adelaide: condensation or crystallization from melt? (abstract). Meteorit. Planet. Sci. 36 (Suppl.), A105.

Krot, A.N., Ulyanov, A.A., Meibom, A., Keil, K., 2001b. Forsterite-rich accretionary rims around Ca, Al-rich inclusions from the reduced CV3 chondrite Efremovka. Meteorit. Planet. Sci. 36, 611–628.

Krot, A.N., McKeegan, K.D., Russell, S.S., Meibom, A., Weisberg, M.K., Zipfel, J., Krot, T.V., Fagan, T.J., Keil, K., 2001c. Refractory Ca, Al-rich inclusions and Al-diopside-rich chondrules in the metal-rich chondrites Hammadah al Hamra 237 and QUE 94411. Meteorit. Planet. Sci. 36, 1189–1217.

Krot, A.N., Hutcheon, I.D., Huss, G.R., 2001d. Aluminum-rich chondrules and associated refractory inclusions in the unique carbonaceous chondrite Adelaide (abstract). Meteorit. Planet. Sci. 36 (Suppl.), A105–A106.

Krot, A.N., Petaev, M.I., Meibom, A., Keil, K., 2001e. In situ growth of Ca-rich rims around Allende dark inclusions. Geochem. Int. 36, 351–368.

Krot, A.N., Keil, K., 2002. Anorthite-rich chondrules in CR and CH carbonaceous chondrites: genetic link between Ca, Al-rich inclusions and ferromagnesian chondrules. Meteorit. Planet. Sci. 37, 91–111.

Krot, A.N., Meibom, A., Weisberg, M.K., Keil, K., 2002a. The CR chondrite clan: implications for early solar system processes. Meteorit. Planet. Sci. 37, 1451–1490.

Krot, A.N., McKeegan, K.D., Leshin, L.A., MacPherson, G.J., Scott, E.R.D., 2002b. Existence of an ^{16}O-rich gaseous reservoir in the solar nebula. Science 295, 1051–1054.

Krot, A.N., Hutcheon, I.D., Keil, K., 2002c. Anorthite-rich chondrules in the reduced CV chondrites: evidence for complex formation history and genetic links between CAIs and ferromagnesian chondrules. Meteorit. Planet. Sci. 37, 155–182.

Krot, A.N., Petaev, M.I., Itoh, S., Fagan, T.J., Yurimoto, H., Russell, S.S., 2003a. Amoeboid olivine aggregates in carbonaceous chondrites: records of nebular and asteroidal processes (abstract). Goldschmidt Conference. Geochim. Cosmochim. Acta 67, A237.

Krot, A.N., Petaev, M.I., Russell, S.S., Itoh, S., Fagan, T.J., Yurimoto, H., Keil, K., 2003b. Amoeboid olivine aggregates in primitive carbonaceous chondrites: records of high-temperature nebular processing (abstract). Meteorit. Planet. Sci. 38 (Suppl.), A74.

Krot, A.N., Hutcheon, I.D., Brearley, A.J., Pravdivtseva, O.V., Petaev, M.I., Hohenberg, C.M., 2003c. Timescales for secondary alteration of chondritic meteorites. In: Lauretta, D., Leshin, L.A., MySween Jr., H.Y. (Eds.), Meteorites and the Early Solar System II. University of Arizona Press (submitted).

Krot, A.N., Fagan, T.J., Keil, K., McKeegan, K.D., Sahijpal, S., Hutcheon, I.D., Petaev, M.I., Yurimoto, H., 2004a. Ca, Al-rich inclusions, amoeboid olivine aggregates, and Al-rich chondrules from the unique carbonaceous chondrite Acfer 094: I. Mineralogy and petrology. Geochim. Cosmochim. Acta 68, 2167–2184.

Krot, A.N., Petaev, M.I., Bland, P.A., 2004b. Multiple formation mechanisms of ferrous olivine in CV carbonaceous chondrites during fluid-assisted metamorphism. Proc. NIPR Symp. Evolution of solar system materials: A new perspective from Antarctic meteorites, Tokyo, Japan (in press).

Krot, A.N., MacPherson, G.J., Ulyanov, A.A., Petaev, M.I., 2004c. Fine-grained, spinel-rich inclusions from the reduced CV chondrites Efremovka and Leoville: I. Mineralogy, petrology, and bulk chemistry. Meteorit. Planet. Sci. (in press).

Krot, A.N., Fagan, T.J., Yurimoto, H., Petaev, M.I., 2004d. Origin of low-Ca pyroxene in amoeboid olivine aggregates: Evidence from oxygen isotopic compositions. Geochim. Cosmochim. Acta (in press).

Krot, A.N., Petaev, M.I., Yurimoto, H., 2004e. Amoeboid olivine aggregates with low-Ca pyroxenes: a genetic link between refractory inclusions and chondrules? Geochim. Cosmochim. Acta 68, 1923–1941.

Krot, A.N., Libourel, G., Goodrich, C.A., Petaev, M.I., 2004f. Silica-rich igneous rims around magnesian chondrules in CR carbonaceous chondrites: evidence for fractional condensation during chondrule formation. Meteorit. Planet. Sci. (in revision).

MacPherson, G.J., Huss, G.R., 2003. Petrogenesis of Al-rich chondrules: evidence from bulk compositions and phase equilibria. Geochim. Cosmochim. Acta (in revision).

MacPherson, G.J., Krot, A.N., 2002. Distribution of Ca–Fe-silicates in CV3 chondrites: possible controls by parent body compaction. Meteorit. Planet. Sci. 37 (Suppl.), A91.

MacPherson, G.J., Hashimoto, A., Grossman, L., 1985. Accretionary rims on inclusions in the Allende meteorite. Geochim. Cosmochim. Acta 49, 2267–2279.

MacPherson, G.J., Wark, D.A., Armstrong, J.T., 1988. Primitive material surviving in chondrites: refractory inclusions. In: Kerridge, J.F., Matthews, M.S. (Eds.), Meteorites and the Early Solar System. University of Arizona Press, Tucson, pp. 746–807.

MacPherson, G.J., Davis, A.M., Zinner, E.K., 1995. The distribution of aluminum-26 in the early solar system. Meteorit. 30, 365–386.

McKeegan, K.D., Leshin, L.A., MacPherson, G.J., 1998. Oxygen-isotopic stratigraphy in a Vigarano type A calcium-aluminum-rich inclusion (abstract). Meteorit. Planet. Sci. 33 (Suppl.), A102–A103.

McSween Jr., H.Y., 1977. Chemical and petrographic constraints on the origin of chondrules and inclusions in carbonaceous chondrites. Geochim. Cosmochim. Acta 41, 1843–1860.

Newton, J., Bischoff, A., Arden, J.W., Franchi, I.A., Geiger, T., Greshake, A., Pillinger, C.T., 1995. Acfer 094, a uniquely primitive carbonaceous chondrite from the Sahara. Meteoritics 30, 47–56.

Ohnishi, I., Tomeoka, K., 2002. Dark inclusions in the Mokoia CV3 chondrite: evidence for aqueous alteration and subsequent thermal and shock metamorphism. Meteorit. Planet. Sci. 37, 1843–1856.

Palme, H., Wark, D.A., 1988. CV-chondrites: high temperature gas–solid equilibrium vs. parent body metamorphism (abstract). Lunar Planet. Sci. XXIX, Lunar Planet. Inst., 897–898.

Petaev, M.I., Wood, J.A., 1998a. The condensation with partial isolation (CWPI) model of condensation in the solar nebula. Meteorit. Planet. Sci. 33, 1123–1137.

Petaev, M.I., Wood, J.A., 1998b. The CWPI model of nebular condensation: effects of pressure on the condensation sequence (abstract). Meteorit. Planet. Sci. 33 (Suppl.), A122.

Petaev, M.I., Wood, J.A., 2000. The condensation origin of zoned metal grains in Bencubbin/CH-like chondrites: thermodynamic model (abstract). Lunar Planet. Sci. XXXI, Lunar Planet. Inst., CD-ROM ♯1608.

Petaev, M.I., Wood, J.A., Meibom, A., Krot, A.N., Keil, K., 2003. The ZONMET thermodynamic and kinetic model of metal condensation in the solar nebula. Geochim. Cosmochim. Acta. 67, 1731–1751.

Podosek, F.A., Cassen, P., 1994. Theoretical, observational, and isotopic estimates of the lifetime of the solar nebula. Meteoritics 29, 6–25.

Pravdivtseva, O.V., Hohenberg, C.M., 2001. The I-Xe system of magnetic fractions from CV3 meteorites (abstract). Lunar Planet. Sci. XXXII, Lunar Planet. Inst., CD-ROM ♯2176.

Pravdivtseva, O.V., Hohenberg, C.M., Meshik, A.P., Krot, A.N., 2001. I-Xe ages of different mineral fractions from Bali and Kaba (CV3) (abstract). Meteorit. Planet. Sci. 36 (Suppl.), A168.

Pravdivtseva, O.V., Krot, A.N., Hohenberg, C.M., Meshik, A.M., Weisberg, M.K., Keil, K., 2003a. The I-Xe record of alteration in the Allende CV chondrite. Geochim. Cosmochim. Acta 67, 5011–5027.

Pravdivtseva, O.V., Hohenberg, C.M., Meshik, A.M., Krot, A.N., Brearley, A.J., 2003b. I-Xe age of the dark inclusions from the reduced CV3 chondrites Leoville, Efremovka, and Vigarano (abstract). Meteorit. Planet. Sci. 38 (Suppl.), A140.

Robie, R.A., Hemingway, B.S., 1995. Thermodynamic properties of minerals and related substances at 298.15 K and 1 bar (10^5 Pascals) pressure and at higher temperatures. USGS Bulletin 2131.

Rubin, 1984. Coarse-grained chondrule rims in type 3 chondrites. Geochim. Cosmochim. Acta 48, 1779–1789.

Rubin, A.E., 1998. Correlated petrologic and geochemical characteristics of CO3 chondrites. Meteorit. Planet. Sci. 33, 385–391.

Russell, S.S., Huss, G.R., Fahey, A.J., Greenwood, R.C., Hutchison, R., Wasserburg, G.J., 1998. An isotopic and petrologic study of calcium-aluminum-rich inclusions from CO3 meteorites. Geochim. Cosmochim. Acta 62, 689–714.

Russell, S.S., Krot, A.N., Jeffries, T.E., Ulyanov, A.A., 2003. Rare earth element systematics of fine-grained calcium–aluminum-rich inclusions and amoeboid olivine aggregates from Efremovka (CV3) (abstract). Lunar Planet. Sci. XXXIV, Lunar Planet. Inst., CD-ROM ♯1631.

Sack, R.O., Ghiorso, M.S., 1994. Thermodynamics of multicomponent pyroxenes. III. Calibration of $Fe^{2+}(Mg)_{-1}$, $TiAl_2(MgSi_2)_{-1}$, $TiFe^{3+}_2(MgSi_2)_{-1}$, $AlFe^{3+}(MgSi)_{-1}$, $NaAl(Ca,Mg)_{-1}$, $Al_2(MgSi)_{-1}$ and $Ca(Mg)_{-1}$ exchange reactions between pyroxenes and silicate melts. Contrib. Mineral. Petrol. 118, 271–296.

Sheng, Y.J., Hutcheon, I.D., Wasserburg, G.J., 1991. Origin of plagioclase-olivine inclusions in carbonaceous chondrites. Geochim. Cosmochim. Acta 55, 581–599.

Shu, F.H., Shang, H., Gounelle, M., Glassgold, A.E., Lee, T., 2001. The origin of chondrules and refractory inclusions in chondritic meteorites. Astrophys. J. 548, 1029–1070.

Simon, S.B., Davis, A.M., Grossman, L., McKeegan, K.D., 2002. A hibonite-corundum inclusion from Murchison: a first generation condensate from the solar nebula. Meteorit. Planet. Sci. 37, 533–548.

Yoneda, S., Grossman, L., 1995. Condensation of $CaO–MgO–Al_2O_3–SiO_2$ liquids from cosmic gases. Geochim. Cosmochim. Acta 59, 3413–3444.

Wark, D.A., Lovering, J.F., 1977. Marker events in the early evolution of the solar system: evidence from rims on Ca–Al-rich inclusions from carbonaceous chondrites. Proc. Lunar Planet. Sci. Conf. 8, 95–112.

Wasson, J.T., Yurimoto, H., Russell, S.S., 2001. ^{16}O-rich melilite in CO3.0 chondrites: possible formation of common, ^{16}O-poor melilite by aqueous alteration. Geochim. Cosmochim. Acta 65, 4539–4549.

Weber, D., Bischoff, A., 1997. Refractory inclusions in the CR chondrite Acfer 059—El Djouf 001: petrology, chemical composition, and relationship to inclusion populations in other types of carbonaceous chondrites. Chem. Erde 57, 1–24.

Weber, D., Zinner, E., Bischoff, A., 1995. Trace element abundances and magnesium, calcium, and titanium isotopic compositions of grossite-containing inclusions from the carbonaceous chondrite Acfer 182. Geochim. Cosmochim. Acta 59, 803–823.

Weisberg, M.K., Prinz, M., 1998. Fayalitic olivine in CV3 chondrite matrix and dark inclusions: a nebular origin. Meteorit. Planet. Sci. 33, 1087–1111.

Weisberg, M.K., Prinz, M., Clayton, R.N., Mayeda, T.K., 1997. CV3 chondrites; three subgroups, not two (abstract). Meteorit. Planet. Sci. 32 (Suppl.), 138–139.

Weisberg, M.K., Prinz, M., Clayton, R.N., Mayeda, T.K., Sugiura, N., Zashu, S., Ebihara, M., 2001. A new metal-rich chondrite grouplet. Meteorit. Planet. Sci. 36, 401–418.

Weisberg, M.K., Connolly Jr., H.C., Ebel, D.S., 2003. Petrology and origin of amoeboid olivine aggregates in CR chondrites. Geochim. Cosmochim. Acta (in revision).